Icosahedral clusters, icosaheral order and stability of quasicrystals—a view of metallurgy

2008 Sci. Technol. Adv. Mater. 9 013008

(http://iopscience.iop.org/1468-6996/9/1/013008)

IOP PUBLISHING SCIENCE AND TECHNOLOGY OF ADVANCED MATERIALS

Sci. Technol. Adv. Mater. **9** (2008) 013008 (20pp) doi:10.1088/1468-6996/9/1/013008

TOPICAL REVIEW

Icosahedral clusters, icosaheral order and stability of quasicrystals—a view of metallurgy*

An Pang Tsai

Institute of Multidisciplinary Research for Advanced Materials, Tohoku University, Sendai 980-8577, Japan and National Institute for Materials Science, 305-0047 Tsukuba, Japan

E-mail: aptsai@tagen.tohoku.ac.jp

Received 9 October 2007
Accepted for publication 15 January 2008
Published 25 April 2008
Online at stacks.iop.org/STAM/9/013008

Abstract

We review the stability of various icosahedral quasicrystals (iQc) from a metallurgical viewpoint. The stability of stable iQcs is well interpreted in terms of Hume-Rothery rules, i.e. atomic size factor and valence electron concentration, e/a. For metastable iQcs, we discuss the role of phason disorder introduced by rapid solidification, in structural stability and its interplay with chemical order and composition.

Keywords: stable quasicrystal, isodahedral cluster, valence concentration, phason disorder, icosahedral order

1. Introduction

A diffraction pattern indicating icosahedral symmetry, long forbidden in traditional crystallography, of Al–Mn alloy prepared by a rapid cooling technique from the melt, had inspired the world of solid state science [1]. Meanwhile, together with icosahedral symmetry, the new phase generates a nonperiodic array of diffraction peaks in the diffraction pattern, indicating an aperiodic arrangement of atoms. Traditionally, a crystalline structure is defined by a periodic repetition of a unit cell, and the periodicity is another definition for translational symmetry, the strictest form of long-range order [2]. On the other hand, an icosahedron is locally the most densely packed arrangement but an icosahedral symmetry is incompatible with the translational symmetry because the icosahedral motif alone cannot completely fill space in three dimensions. Therefore, it was believed to be impossible that a long-range order with icosahedral symmetry would be formed in a realistic matter.

Nowadays, more than one hundred alloys [3, 4] have been verified to be stable icosahedral quasicrystals (iQcs) and that iQcs exist in the equilibrium phase diagrams. Undoubtedly, the quasicrystal is no longer a unique form of solid; it exists universally in many metallic alloys and some polymers [5]. Except for the Al–Li–Cu system, all the stable iQcs are well ordered in structure and almost free of defects and disorder, as evidenced by x-ray and electron diffraction studies where stable iQcs reveal peak widths as sharp as those of perfect crystals such as Si, which enable ones to study the structure in detail. In principle, the stable iQcs are realized as a new form of Hume-Rothery electron compounds [6] in which the valence electron concentration is particularly important. On the other hand, since a number of stable iQcs have been found, less attention has been paid to the metastable ones owing to their intrinsic disorder and instability. However, the intrinsic disorder is generally created during the growth processes, and partly contains structural characteristics of the liquid state. The structure of metastable iQc is believed to contain structural units which also exist in the stable iQc and the liquid state. Therefore, the metastable iQc may be regarded as an intermediate between the latter two states, and by incorporating structural information of the three states, one may gain insight as to why Nature prefers the quasicrystalline structure.

* Invited paper.

In this article, we overview the stability of quasicrystals in light of physical metallurgy and in relation to phason disorder. The stability of iQc has generally been discussed in terms of electron structure, i.e. the interaction of Fermi spheres and rillouin zones, but because of the page limitation, we do not go into the details of this topic in this article. The intention of this article is to overview the stability of iQcs in a unique way such that we cover stable and metastable iQcs. The article is organized into three parts. First, we briefly describe how to obtain a one-dimensional quasicrystal by means of the projection method. By choosing the proper conditions, one can obtain a random quasicrystal or a long periodic crystal which could be viewed as a kind of 'quasi-quasicrystal', where the term of phason strain has a key role in the interaction with the quasiperiodic structure. Theoretically, three possible models are derived by the projection method: the perfect quasicrystal, the quasicrystal with linear strain and the quasicrystal with random strain. We use three real examples that are described by the three respective models, and discuss their stability separately.

Most of the metastable iQcs obtained by rapid solidification are quasicrystals with linear phason strain, and those obtained by the crystallization of glass states are quasicrystals with random strain. Structures of metastable iQcs will be considered in light of quenched-in strains. The roles of chemical order and chemical composition in structural stability will be discussed. For perfect quasicrystals, most stable iQcs are described by this model and their stability is elucidated in terms of Hume-Rothery rules, e.g. valence electron concentration (e/a) and atomic size factor.

2. Structural description of iQc

2.1. Structures in projection scheme

The term of 'phason' appeared in the literature [7] soon after the discovery of the quasicrystal. Theoretical treatments of highly ordered quasicrystals introduce two unit cells with different shapes into tilings [8, 9], like those described in Penrose tiling. Such arrangements in a given number of dimensions (D) have $2 \times$ D degrees of freedom, instead of the $1 \times$ D for crystals. The additional degrees of freedom are associated with the relative phase of the two different unit cells, and allow a new hydrodynamic variable to be identified, the 'phason' vector. This vector can be continuously varied in analogy to the phonon (translation vector) found for both crystals and quasicrystals. Just as the phonon variable leads to long wavelength and low energy distortion of crystals, the phason variable in quasicrystals leads to a second type of distortion, 'phason strain' or 'phason disorder'. Such phason strain is expected in three-dimensional tiling with two definite building blocks. Here, details of the theoretical background of phason strain are not given but the resultant effect of phason strains representing in diffractions observed in the samples prepared by different processes, will be discussed. In order to capture the essential concept of phason strain, we use a simple projection method to describe it, although it does not give symmetry elements that are found in three-dimensional cases.

Figure 1(a) is a schematic projection from two-dimensions to one-dimension of a Fibonacci sequence illustrating the different kinds of phason disorder leading to different diffraction effects. Let a two-dimensional lattice points sit at the corners of squares in a grid. Then, we design a strip with a slope of an irrational number $\tan^{-1}(1/\tau)$, where τ is the golden mean, $(1+\sqrt{5})/2$, with respect to the lattice, and let lattice points covered by the strip project onto a line that is parallel to the strip; the projected points will divide the line into a quasiperiodic sequence of long (L) and short (S) segments. This sequence is called a Fibonacci sequence and is exactly a one-dimensional quasicrystal if we imagine that an atom sits at each of the points divide the line into long and short segments. The diffraction pattern derived from the quasiperiodic sequence consists of a dense set of weak and strong peaks [10] and is similar to that obtained from stable $Zn_{80}Mg_5Sc_{15}$ iQc [11]. Using a similar approach to that of diffraction experiments, one can solve the structure of iQc [12, 13], which is described as a three-dimensional cut through an abstract six-dimensional lattice. This kind of cut leads to a space filling with specific units arranged in an aperiodic way with icosahedral symmetry [14, 15]. This is a framework structure of the iQc. In the ideal case, there is no phason disorder, and in fact, no visible phason disorder was observed in the stable iQcs [16]. A twofold electron diffraction pattern obtained from such a stable iQc, together with its line profile along a twofold direction, are displayed in figure 1(a), which shows that the lattice spacing inflates with a τ scaling. Most stable iQcs are free of phason disorder and generally have a narrow composition range, therefore their stability is elucidated in terms of the Hume-Rothery rules, as will be described in section 4.

The second case is one in which the slope of the strip with respect to the lattice is $\tan^{-1}(1/2)$, which is a rational number. The projected points will divide the line into a sequence of two long and one short segment, i.e. a sequence of LLSLLSLLS .... This sequence gives a diffraction pattern with a similar distribution of peaks to those of the quasiperiodic sequence but nevertheless, it is a periodic sequence. Consequently, this is a crystal with a periodicity of LLS, and by tilting the strip to a slope toward an irrational number, one can obtain a sequence with longer periodicity, e.g. LLSLS, LLSLLSLS. Note that the ratios of n_L/n_S are 2/1, 3/2, 5/3.... If the slope of the strip is the irrational number $\tan^{-1}(1/\tau)$, n_L/n_S is τ the sequence will be quasiperiodic. A sequence with rational ratios of n_L/n_S is called an approximant. A higher order (with n_L/n_S close to τ) approximant can be described as a quasicrystal with a linear phason. Note that two sequences are surrounded by two dotted lines on the left-hand side in figures 1(a) and (b). The sequence is LSL in a perfect quasicrystal but it is LLS in the approximant where the sequence changes by a flip between S and L arising from the projection of a different lattice point. This flip called phason flip, is a flipping of tiles in two-dimensions or three-dimensions. The illustration given in figure 1(b) is an example of the 2/1 approximant in the In–Ag–Yb system [17]. In three-dimensions, the 2/1 approximant is a cubic structure that has an electron diffraction pattern (along a pseudo

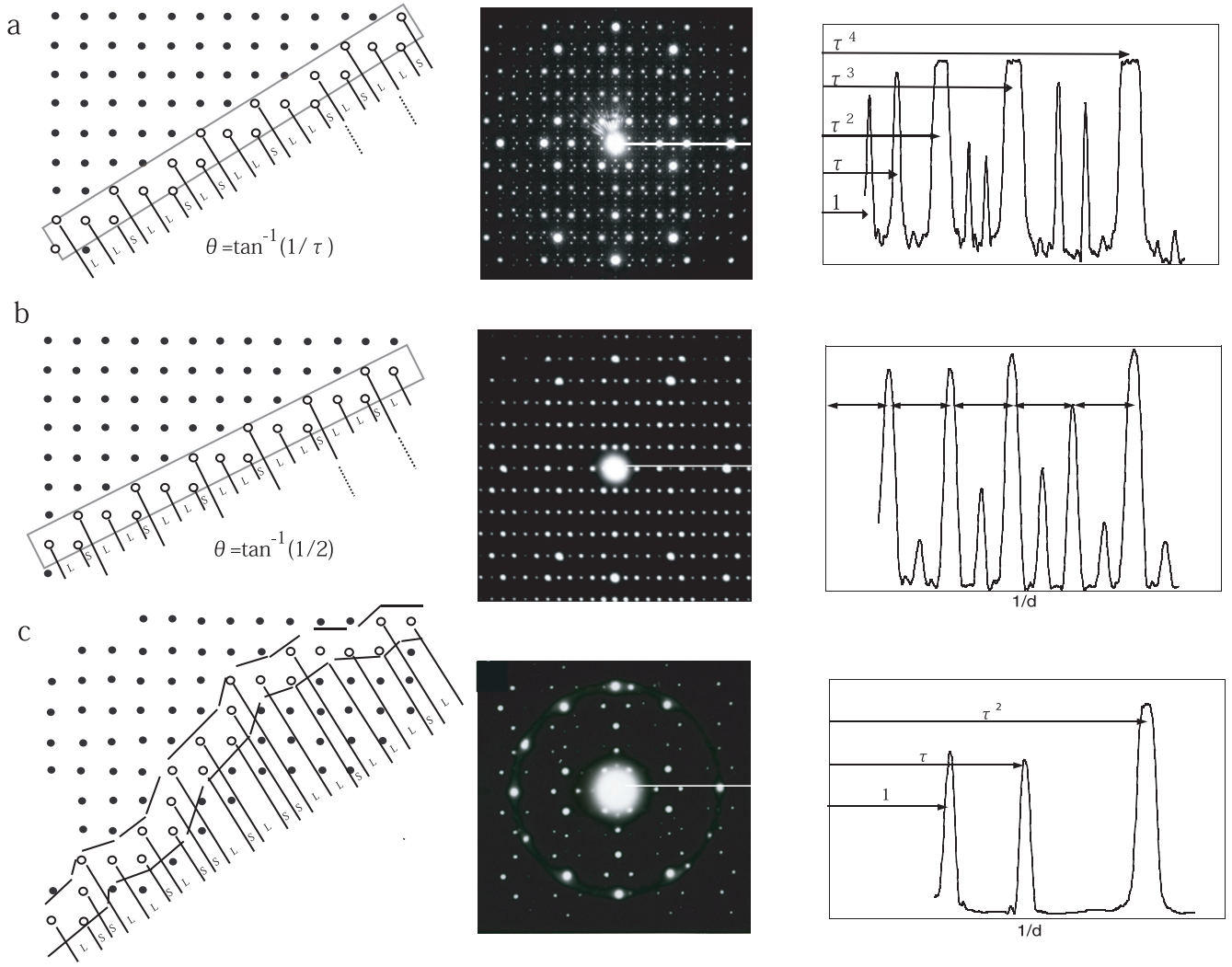

Figure 1. The projection method with different slopes of the strip for different sequences: (a) the Fibonacci sequence projected from a strip with slope of $\tan^{-1}(1/\tau)$, (b) the LLS periodic sequence projected from a strip with slope of $\tan^{-1}(1/2)$, (c) a random sequence projected from a random work strip with overall slope close to $\tan^{-1}(1/\tau)$. Electron diffraction patterns: (a) twofold from the stable $Zn_{80}Mg_5Sc_{15}$ iQc, (b) (100) from the $In_{44}Ag_{41}Yb_{15}$ 2/1 approximant, (c) twofold from the metastable $Al_{75}Cu_{15}V_{10}$ iQc. The line profiles obtained along twofold axes indicated with white lines are shown on the right-hand side.

twofold axis) and the line profile shown on the right-hand side of figure 1(b).

Another extreme example has long and short segments arranged in a completely irregular fashion with the resultant sequence being random, as shown in figure 1(c). Note that the short-segment pair of SS, which is not allowed in the quasiperiodic sequence, appears in the random sequence. To obtain this sequence, a corresponding strip of a random walk is used. If the average slope of the strip of the random walk is maintained at around $\sim\tan^{-1}(1/\tau)$, the random sequence will give rise to a diffraction pattern that is quite similar to the pattern obtained from the original quasiperiodic sequence. The diffraction patterns of the random sequence are found at the same positions as those from the quasiperiodic sequence but are broader. This corresponds to a quasicrystal with random phason disorder, which is clearly observed in the iQcs obtained by the crystallization of amorphous phases. One such electron diffraction pattern and its line profile are shown in figure 1(c). Only the more intense peaks remain. Nevertheless, the existence of relatively sharp diffraction peaks from the random sequence indicates that quasiperiodicity can survive disorder.

Figure 1 shows three structures derived from the projection method, a perfect quasiperioidc structure, a longer but periodic structure and an averaged quasiperiodic structure with intrinsic disorder, that are observed in real iQcs. For the perfect quasiperiodic structure, we will deal with Hume-Rothery rules, in particular, electron valency. We will then describe the last two structures associated with phason disorder and discuss the effects of the compositions and chemical order on phason disorder.

2.2. iQcs with extinction rules

The stable iQcs studied by electron diffraction analysis exhibit reflections arranged quasiperiodically in three dimensions.

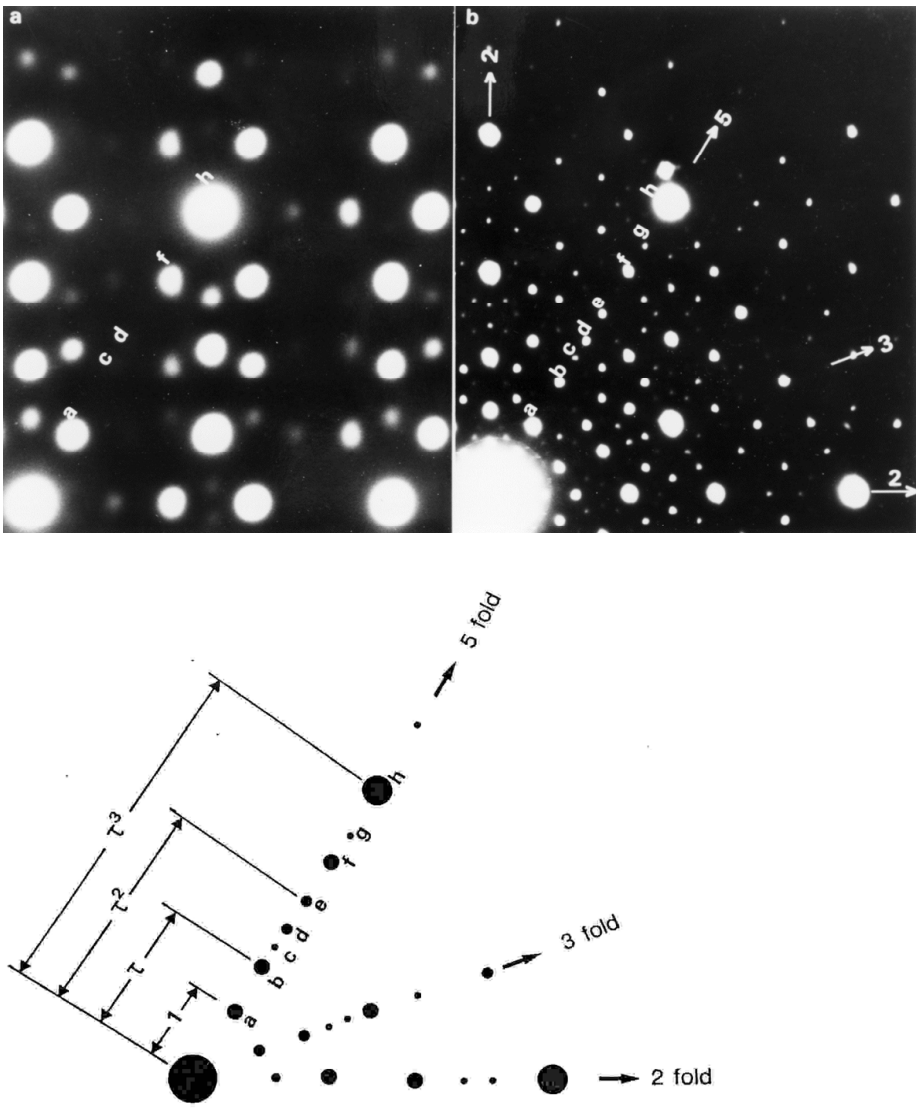

Figure 2. Twofold diffraction patterns of (a) P-type and (b) F-type iQcs.

The stable iQcs generally have icosahedral symmetry revealing diffraction patterns of fivefold, threefold and twofold symmetries. It has been shown that there can exist three types of Bravais lattices in three dimensions consistent with the icosahdral symmetry [18]. The three lattices correspond to the primitive, body-centered and face-centered hypercubes in six dimensions [19]. The primitive and face-centered iQcs have been verified in several alloys. These two types of iQcs can be distinguished by their twofold patterns. Figure 2 shows twofold patterns of the primitive (P-type) and face-centered (F-type) iQcs indexed along the fivefold direction. Along this fivefold direction, the distance between the reflections shows an inflation by τ^3 for the P-type iQc and by τ for the F-type iQc [20, 21]. The indexing of these reflections is shown in table 1. The six-dimensional indices $(n_1, n_2, n_3, n_4, n_5, n_6)$ of these reflections have all combinations of integers n_i for the P-type iQc, while the superlattice reflections (at τ ratios) in the F-type iQc have only odd integers. In the earlier period, the P-type iQc was only observed in samples with a large amount of intrinsic disorder, and it was suspected that the superlattice reflections that characterize the F-type structure may be hidden underneath the disorder. This suspicion has been clarified by the discovery of a group of iQcs in the Cd–Yb class [22], several iQcs of which reveal P-type structure with high structural perfection.

Table 1. Indexing of reflections in figure 2.

Reflection	Indices	
	Elser	Cahn
a	(100000)	(2/0 0/2 0/0)
b	1/2(111111)	(0/2 2/2 0/0)
c	(200000)	(4/0 0/4 0/0)
d	(011111)	(2/4 4/2 0/0)
e	1/2(311111)	(2/2 2/4 0/0)
f	(111111)	(0/4 4/4 0/0)
g	1/2(511111)	(4/2 2/6 0/0)
h	(211111)	(2/4 4/6 0/0)
i	(311111)	(4/4 4/8 0/0)

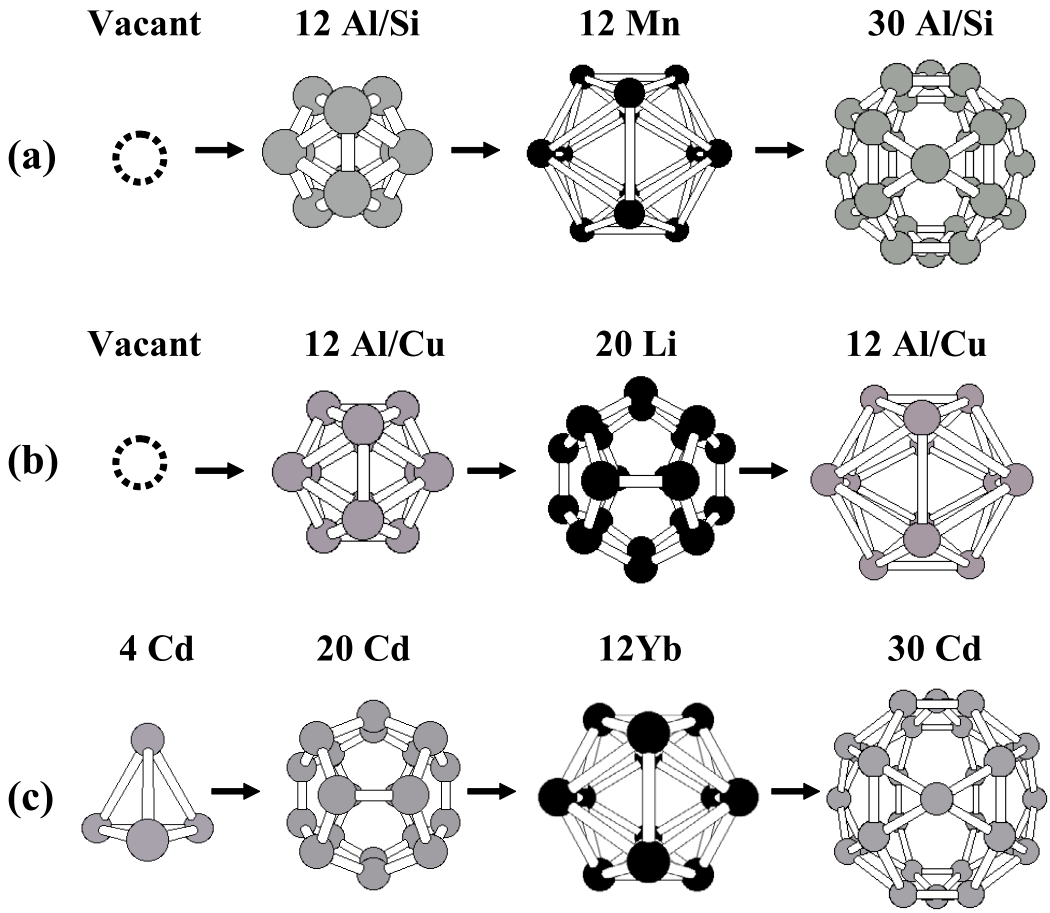

Figure 3. Concentric structures of three types of icosahedral clusters derived from three 1/1 approximants of quasicrystals. (a) The Al–Mn–Si class or Mackay icosahedral cluster: the center is vacant, the 1st shell is an Al/Si icosahedron, the 2nd shell is a Mn icosahedron, and the 3rd shell is an Al/Si icosidodecahedron. (b) The Zn–Mg–Al class or Bergman cluster: an example is R-AlLiCu: the center is vacant, the 1st shell is an Al/Cu icosahedron, the 2nd shell is a Li dodecahedron, the 3rd shell is a larger Al/Cu icosahedron. (c) The Cd–Yb class: the center is a Cd tetrahedron, the 1st shell is a Cd dodecahedron, the 2nd shell is a Yb icosahedron, and the 3rd shell is a Cd icosidodecahedron.

2.3. iQcs with different clusters

Long before the discovery of iQcs, it was already known that although fivefold and icosahedral symmetry is forbidden in the presence of two- and three-dimensional translation groups, local icosahedral arrangements of atoms in crystals are possible. Indeed, this is fairly common in some complex metallic alloys. Many such alloys are now called 'approximants' [23]. As mentioned in section 2.1, the approximant can be generated by a rational cut through high-dimensional space, and hence an approximant and an iQc is related in structure through 'linear phason strain', as described in figure 1(b). It is described that an identical icosahedral cluster exists in both the iQc and the corresponding approximant but it is in a quasiperiodic arrangement for the former and a periodic arrangement for the latter [23]. Indeed, the electron diffraction pattern in figure 1(b) is a twofold pattern of a 2/1 approximant.

Approximants are important for understanding the structure of the iQc since the structures of approximants have been well defined, which is very helpful in obtaining a primary structure model. The iQcs can be classified into three classes according to hierarchic structures of icosahedral clusters derived from their counterpart approximants: the Al–Mn–Si [23, 24] class, the Mg–Al–Zn [25, 26] class and the Cd–Yb [22, 27] class. The structures of the atomic shells for the three classes are shown in figure 3. It has been recognized that two complex compounds, whose structures are well known, α-$Mn_{12}(Al, Si)_{57}$ [24] and $Mg_{32}(Al, Zn)_{49}$ [25], were indeed approximants of the iQcs in the Al–Mn–Si class and the Mg–Al–Zn class, respectively. The former is also called the Mackay cluster and the latter is known as the Bergman cluster. Each of these two structures has a bcc packing of clusters consisting of three concentric atomic shells with icosahedral symmetry, as shown in figures 3(a) and (b). The stable iQcs found in Al–Cu–Fe and Al–Pd–Mn alloys were grouped into the Al–Mn–Si class and their corresponding approximants were found in the same alloy systems but at compositions deviating from those of iQcs [28, 29]. On the other hand, stable iQcs in the Zn–Mg–RE (RE: rare-earth metals) systems were grouped into the Mg–Al–Zn class, but no corresponding approximants were found in this system.

The third class of Cd–Yb is related to the Cd_6Yb approximant, which has a bcc packing of identical icosahedral

clusters. In the core of each cluster, there is a tetrahedron created by four positionally disordered Cd atoms, as shown in figure 3(c), which breaks the icosahedral symmetry. The iQcs and approximants having identical cluster structures have been found in several alloys [11, 30, 31]. The iQcs and approximants of the Cd–Yb class have been found in a large number of alloys and constitute the largest of the three classes of iQcs.

3. Metastable iQcs with quenched-in phason disorder

Many efforts were made to find new iQcs by substituting Mn with other transition metals or by adding metalloids, soon after the discovery of iQc. These attempts did lead to the discovery of a number of metastable iQcs. It was also found that the equilibrium states of the metastable iQcs are generally crystalline compounds or approximants. As described above, an approximant is a compound whose composition and structural unit are very similar to that of the corresponding iQcs, but is nevertheless a crystal. The structures of approximants have been well defined and have been analyzed locally as icosahedral clusters [23–26]. Since the iQcs could be obtained by conducting rapid solidification from the crystalline approximants, the quasicrystalline phases were realized to be energetically metastable phases with respect to the corresponding crystalline approximant. As a result, the metastable iQcs generally reveal shifts of peak positions or/and broadening of peak widths. Actually, broadening of peak widths in diffraction patterns can arise either from isotropic strains or from a superposition of the shifted peaks produced by large regions containing different average linear strains. Either linear strain or isotropic strain observed in quasicrystals is ‘phason strain’, which is the characteristic disorder for quasicrystals but does not exist in crystals. Phason strains are represented by shifts of peak positions and broadening of peak widths, which strongly depend on the growth process. In this section, we focus on two examples of metastable iQcs formed by different processes; an $Al_{72}Pd_{25}Cr_3$ iQc prepared by liquid quenching that reveals severe linear phason strain and an $Al_{75}Cu_{15}V_{10}$ (or $Al_{55}Si_{25}Mn_{20}$) iQc formed from the amorphous state that shows a high density of random phason disorder, and discuss phason strain in relation to the growth process in 3.1 and 3.2, respectively.

For a fully annealed stable iQc that is almost free of phason disorder, a certain amount of phason disorder can be introduced by liquid quenching. The degree of such quenched-in phason disorder in iQcs differs in different alloy systems, e.g. it is very severe for the Al–Cu–Fe system but not significant for the Al–Pd–Mn system. This difference is discussed in terms of the inherent chemical order in 3.3. By conducting liquid quenching, the iQc is formed in a wide compositional range for the Al–Pd–Mn system, and there is a relationship between composition and phason disorder. This will be discussed in 3.4.

3.1. iQc prepared by rapid solidification (Al–Pd–Cr)

In general, a quasicrystal grain contains phason strain created during the growth process, which, unlike phonon strain, relaxes slowly and is effectively quenched. In a sufficiently large region of a grain, the variations of the phason strain field can be decomposed into an average linear variation, which leads to shifts of the diffraction peaks, and nonlinear modulations, which lead to peak broadening [32]. Actually, neither the peak shift nor peak broadening is solely observed in real samples. They always appear concurrently. Generally, shifts of diffraction peaks are mainly observed in metastable iQcs prepared by melt-spinning, i.e. the linear phason strain is prominent in the samples [33, 34]. Figure 4 is a bright-field image and corresponding selected-area diffraction patterns taken from the areas indicated by circles. Depending on the area, diffraction patterns display different distortion or deviation of reflections. This is particularly clear for the innermost reflections. Shown in figure 5 are the (a) microstructure and (b)–(d) electron diffraction patterns taken along different axes for a melt-spun $Al_{72}Pd_{25}Cr_3$ alloy. The sharp grain boundaries and a large number of striated contrasts within grains are clearly seen in figure 5(a). For example, the grain at the center exhibits striated contrast radiating from right-hand side of the image. It is inferred that crystal growth of the grain originated from the right-hand side and progressed along g-direction (indicated with an arrow) to the upper-left corner. The diffraction patterns of figures 5(b), (c) and (d) were obtained from the area indicated by a white circle by tilting through the appropriate angles to the two-, three- and five-fold orientations. The size of the white circle is the size of the selected area aperture used to obtain diffraction patterns. The diffraction pattern corresponding to figure 5(a) is the twofold pattern shown in figure 5(c). According to this pattern, one can realize that the growth direction (g) is along a fivefold direction of the iQc grain. It is also clear that most of the diffraction spots deviated from ideal positions and formed a jig-zag arrangement of spots that is particularly conspicuous along the growth (fivefold) direction, indicating that phason strain formed during the growth process. The anisotropic phason strain was explained in terms of a strain field, as described in the following.

In general, an iQc is described by three-dimensional quasiperiodic tiling in which two rhombohedra are used to produce a structure with icosahedral symmetry. The treatment of phason strains in the form the density wave of the tiling pictures, and the connection between them have been given in [9]. In the tiling picture, a spatially varying phason strain variable (W) produces flipping between the two rhombohedra. Matching rules governing the spatial arrangement and attachment of edges of the two cells are locally violated, producing misfits. In the mass density wave picture, strains in the iQc produce shifts (ϕ) in the phase of waves [9]

$$\phi = \boldsymbol{U}(\mathbf{x}) \cdot \mathbf{G}_{\parallel} + \boldsymbol{W}(\mathbf{x}) \cdot \mathbf{G}_{\perp}. \quad (1)$$

Here, U is the conventional strain displacement variable and W is taken to be linearly related to the lattice position through

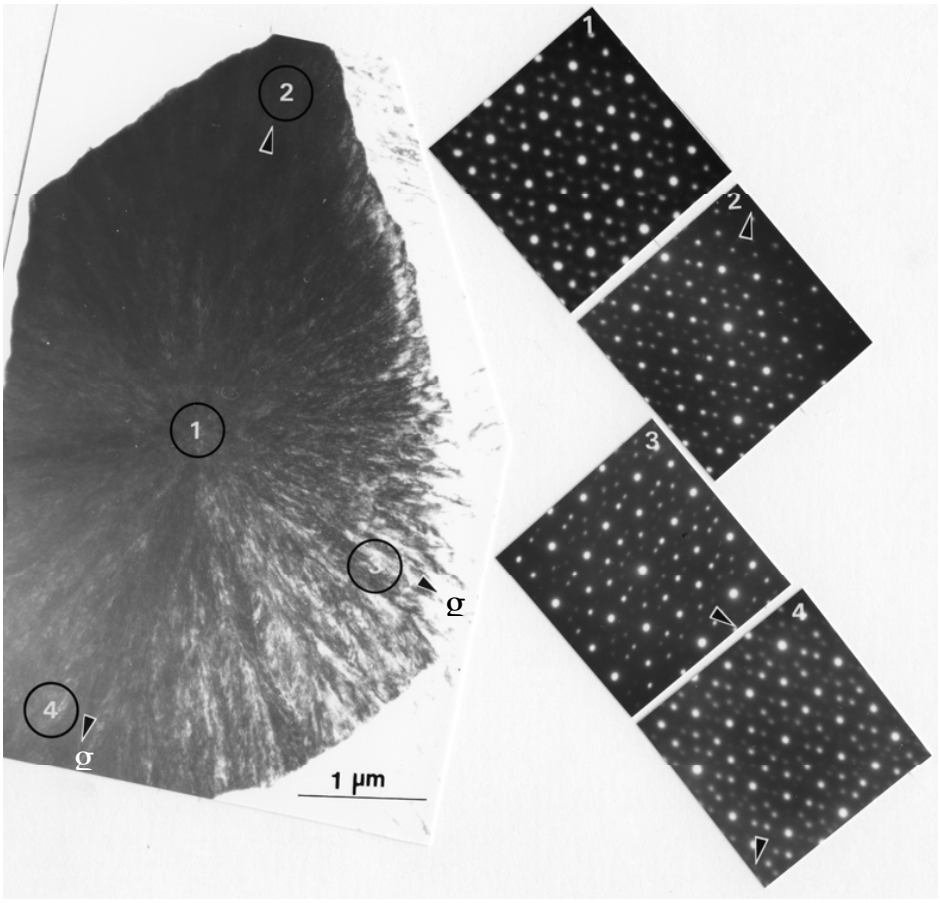

Figure 4. Bright-field image and electron diffraction patterns along fivefold axis obtained from different areas encircled in the image for melt-quenched $Al_{72}Pd_{25}Cr_3$.

a phason strain matrix M [35]. ($U(x)$ and $W(x)$ are taken to be functions of position x in the iQc.)

$$W = x \cdot M. \tag{2}$$

M is a 3×3 matrix with elements m_{ij}. This relationship gives the change in the phason variable over the region of interest. In the Fourier analysis of the mass density, the phason variable shifts the phase of the wave according to

$$e^{ix\cdot G_\parallel + \phi} = e^{ix\cdot(G_\parallel + MG_\perp)}. \tag{3}$$

The second term in the parentheses is the shift in the observed reciprocal lattice wave vector G

$$G = G_\parallel + \Delta G_\perp, \quad \text{where } \Delta G = M \cdot G_\perp. \tag{4}$$

That is each reciprocal lattice point will be shifted, in the presence of phason strain by a vector obtained from the three components ($\mathbf{G}_\perp$) of the rotated six-dimensional vector.

Distortion from icosahedral symmetry in electron diffraction patterns was derived by the method described by Follstaedt and Knapp [36]. The patterns in figures 5(b) through 5(d) were obtained from the same area of a grain after tilting through the appropriate angles to the five-, three- and twofold directions. (A set of x, y and z axes of a reference cube is shown for the patterns indicated by arrows.) Deviations of peaks from ideal positions of perfect icosahedral symmetry are used to estimate the matrix (M) described above. The shifts of weak reflection in the x direction as a result of the nonzero element of $M(m_{11})$ produce clear jogs from straight lines; intense reflections remain more nearly aligned. Here, $\Delta G(= M \cdot G_\perp)$ is the shift of the reflection evaluated from diffraction patterns. It has been discussed that the dependence of the shifts on ΔG in equation (4) indicates that weak reflections will normally be shifted the most since their intensity is inversely proportional to $|\mathbf{G}_\perp|$. Such shifts of the distortion are due to phason strains. On the basis of detailed analysis, the phason strain matrix for the grain, obtained from figures 5(b) through (d), is

$$M = \begin{vmatrix} 0.23 & 0 & 0 \\ 0.001 & 0.095 & 0 \\ 0 & 0 & 0 \end{vmatrix} \sim \begin{vmatrix} 1/\tau^3 & 0 & 0 \\ 0 & 1/\tau^5 & 0 \\ 0 & 0 & 0 \end{vmatrix},$$

where the axes for M are three orthogonal twofold axes, x, y and z, indicated in figure 5(e). In this sample, only one sector of diffraction patterns was examined so that no information on the z-axis is given. In view of the diffraction patterns, the phason strain is not a completely linear but is more complicated. The elongation of reflections along the same direction implies that phason strains with the same matrix tensor but different strength are continuously distributed in the sample. However, they are roughly approximated to linear

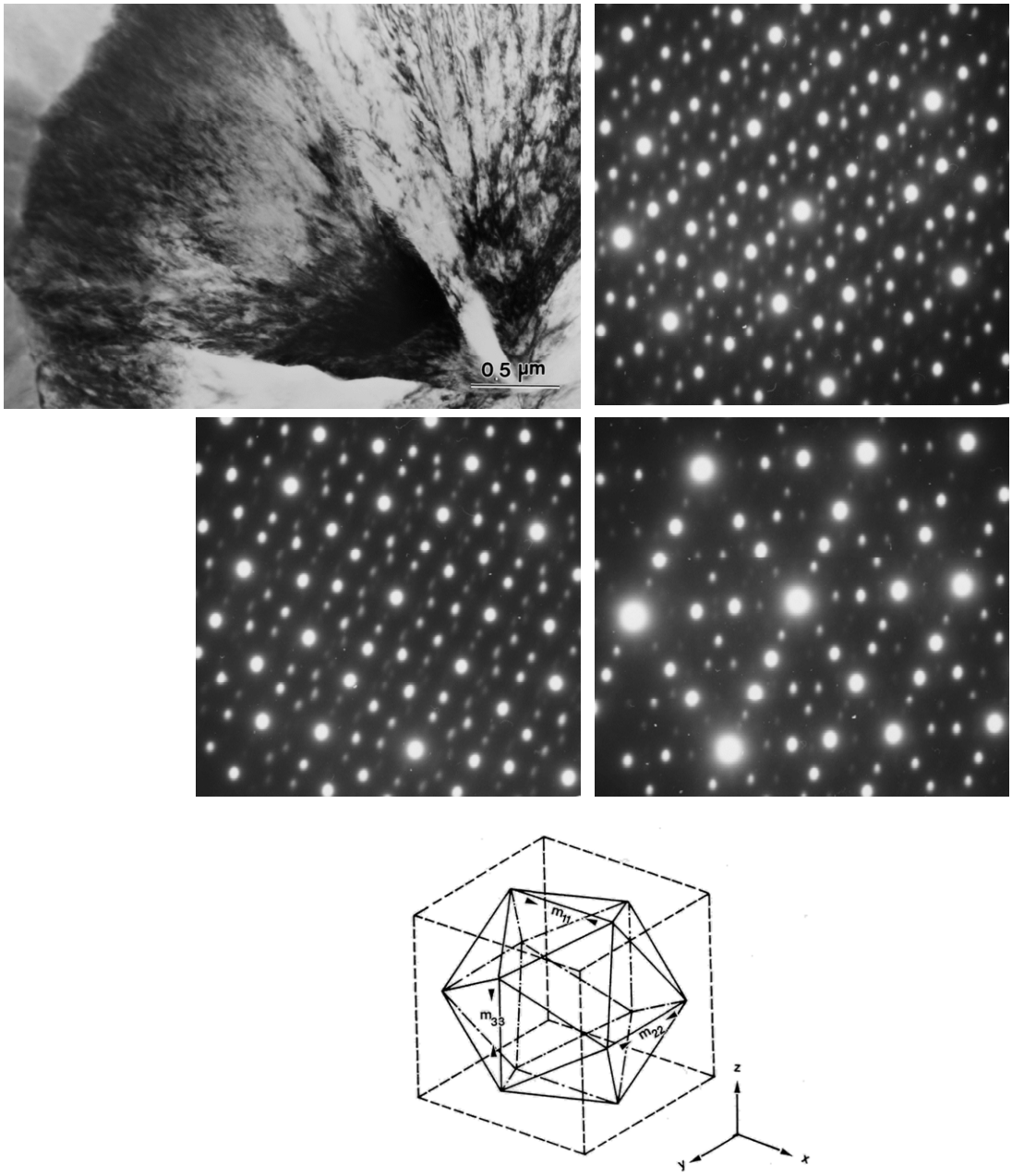

Figure 5. (a) Bright-field image and (b)–(d) electron diffraction patterns taken from the same area along two-, three-, fivefold axes.

phason strains since the estimation of M only has an accuracy of about ± 0.002. In general, the approximant crystalline structure can be interpreted in terms of linear phason strains. The corresponding phason strain matrix for the orthogonal crystal system is given by Mukhopadhyay *et al* [37],

$$M = \begin{vmatrix} m_{11} & 0 & 0 \\ 0 & m_{22} & 0 \\ 0 & 0 & m_{33} \end{vmatrix}$$

with the following conditions

cubic: $m_{11} = m_{22} = m_{33}$
tetragonal: $m_{11} = m_{22} \cdot m_{33}$
orthorhombic: $m_{11} \cdot m_{22} \cdot m_{33}$.

Thus, this result shows that the iQc has a phason strain toward an orthorhombic or a tetragonal crystalline structure with the lattice constants of about 1.23 nm or 3.23 nm, respectively. A metastable orthorhombic Al-Pd with lattice parameters of $a = 2.34$ nm, $b = 1.67$ nm and $c = 1.23$ nm is thought to be an intermediate between a decagonal quasicrystal and the corresponding equilibrium phase [38]. Furthermore, another stable orthorhombic phase with lattice parameters of $a = 1.25$ nm, $b = 3.28$ nm and $c = 2.38$ nm was observed in $Al_{72}Pd_{18}Cr_{10}$ alloy by electron diffraction and high-resolution electron microscopies [39]. $Al_{72}Pd_{18}Cr_{10}$ in the melt-quenched state is an iQc possessing a relatively high crystallinity in comparison with $Al_{72}Pd_{25}Cr_3$ [40, 41]. It is clear that the observed linear phason strains indicate that

evidence of orthorhombic phase still persists in the iQc. Since there is no stable iQc in the Al–Pd–Cr system, the orthorhombic $Al_{72}Pd_{18}Cr_{10}$ [39] is an approximant whose metastable phase is an iQc with a certain amount of disorder including phason strain and defects. When the alloy composition deviates from $Al_{72}Pd_{18}Cr_{10}$, disorder of the obtained iQc upon melt-quenching will increase.

3.2. iQcs formed by crystallization of amorphous phases (Al–Cu–V, Al–Mn–Si)

The structural relationship between liquid and iQc was discussed in terms of the orientational order of icosahedral clusters soon after the discovery of iQcs. A molecular-dynamics simulation of an undercooled Lennard–Jones liquid [42] revealed a structure with an icosahedral bond orientational order. A comparison of the structure between liquid and iQc gave rise to the idea of an icosahedral glass (IG) model [43, 44], by which the inherent disorder in iQc is interpreted. Although the IG model failed to explain the sharp diffraction peaks observed in several stable iQcs, the idea still prevails that there exists a structural correlation between the amorphous phase and iQcs. The iQcs formed through the crystallization of the amorphous phase were first observed in thin film samples of Al–V and Al–Mn alloys. A single phase of iQc, which is converted from the amorphous phase without a change in composition, was found in Pd–U–Si, Al–Mn–Si and Al–Cu–V alloys [45]. Recently, the crystallization of the amorphous phase to the iQc was also observed in some Zr-based alloys [46]. However, the amorphous phases in these alloys do not completely convert to the iQc, i.e. the iQc always coexists with the amorphous phase. Here, we describe the structure of the iQc of this type in $Al_{53}Mn_{20}Si_{27}$ and $Al_{75}Cu_{15}V_{10}$ alloys in relation to phason disorder and compare it with the structure of iQcs obtained by other processes.

The evolution of the structure of the iQc from the amorphous phase for $Al_{53}Mn_{20}Si_{27}$ and $Al_{75}Cu_{15}V_{10}$ alloys is shown in figures 6–8. The kinetics of the transition for both alloys has been clarified to be the nucleation-growth process. A significant feature commonly observed in the two amorphous phases is the presence of a prepeak, at $Q = 15$ and $Q = 16\,\mathrm{nm}^{-1}$, respectively, which is evidence of the chemical short-range order in the sense of compound formation. The interatomic distance corresponding to the prepeak derived using the Ehrenfest relation, $Q_{AB} = 1.23(2\pi/d_{AB})$, is about $\sim$0.48 nm for amorphous $Al_{53}Mn_{20}Si_{27}$ and 0.51 nm for amorphous $Al_{75}Cu_{15}V_{10}$, and is associated with the Mn–Mn correlation ($\sim$ 0.465 nm) in α-AlMnSi [24] for the former and the V–V correlation ($\sim$0.51 nm) in α-AlV [47] for the latter. The Mn–Mn correlation is the distance between Mn–Mn in the Mackay icosahedron verified in α-AlMnSi, and the V–V correlation is the distance between atoms that are located at the centers of icosahedra in α-AlV. A number of x-ray diffraction studies have revealed that the structure of the iQc is identical to that of the amorphous phase within 0.6 nm for $Pd_{60}U_{20}Si_{20}$ [48] and $Al_{75}Cu_{15}V_{10}$ alloys [49]. The results suggest that the icosahedron in

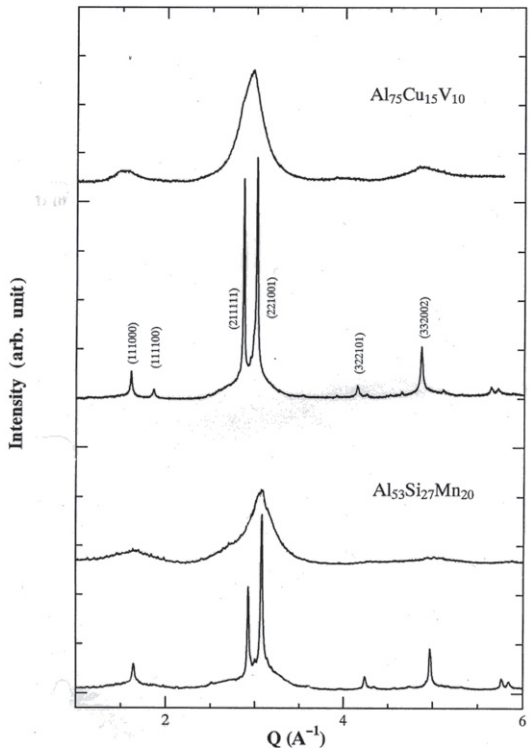

Figure 6. Powder x-ray diffraction patterns as a function of Q ($Q = 4\pi \sin\theta/\lambda$) of as-quenched state and annealed state for $Al_{75}Cu_{15}V_{10}$ and $Al_{53}Si_{27}Mn_{20}$ alloys.

the corresponding intermetallic compound also exists in the amorphous phase and the iQc. However, the iQc in $Al_{53}Mn_{20}Si_{27}$ and $Al_{75}Cu_{15}V_{10}$ alloys is not stable, and transforms to a mixture of crystalline phases at higher temperatures. α-AlMnSi and α-AlV coexist in the mixture of crystalline phases, and thus, the description of the chemical short-range order in these two alloys is reasonable.

As mentioned previously, iQc crystallizes via a nucleation-growth process in which the growth is isotropic and no planar facet is observed, as shown in figures 7 and 8. This morphology is easily explained in terms of the random aggregation of icosahedral clusters. In this way, local icosahedral units are excreted by the attachment of an icosahedron to a randomly chosen vertex or face of the icosahedral seed. To ensure orientational order, adjacent icosahedra are given the same orientation. This idea is supported by the results of high-resolution TEM observation. Figure 9 shows (a) the high-resolution image, (b) the selected-area diffraction pattern taken with the incident beam along the fivefold axis, and (c) the pattern obtained by connecting the bright dots in figure 9(a). The fringes in figure 9(a) exhibit mismatch along various directions, indicating a random distribution of phason disorder. The pattern drawn from the lattice image (figure 9(c)) is a two-dimensional structure consisting of pentagons stuck together, side by side, in a random manner. Besides the 'diamonds' and 'boats' often observed in ideal Penrose tiling, the lattice image reveals unique tear-like or crack-like defects, shown as dark areas, which is similar to the icosahedral glass model pattern derived by simulation. Although the structure of the iQc is highly defective, the

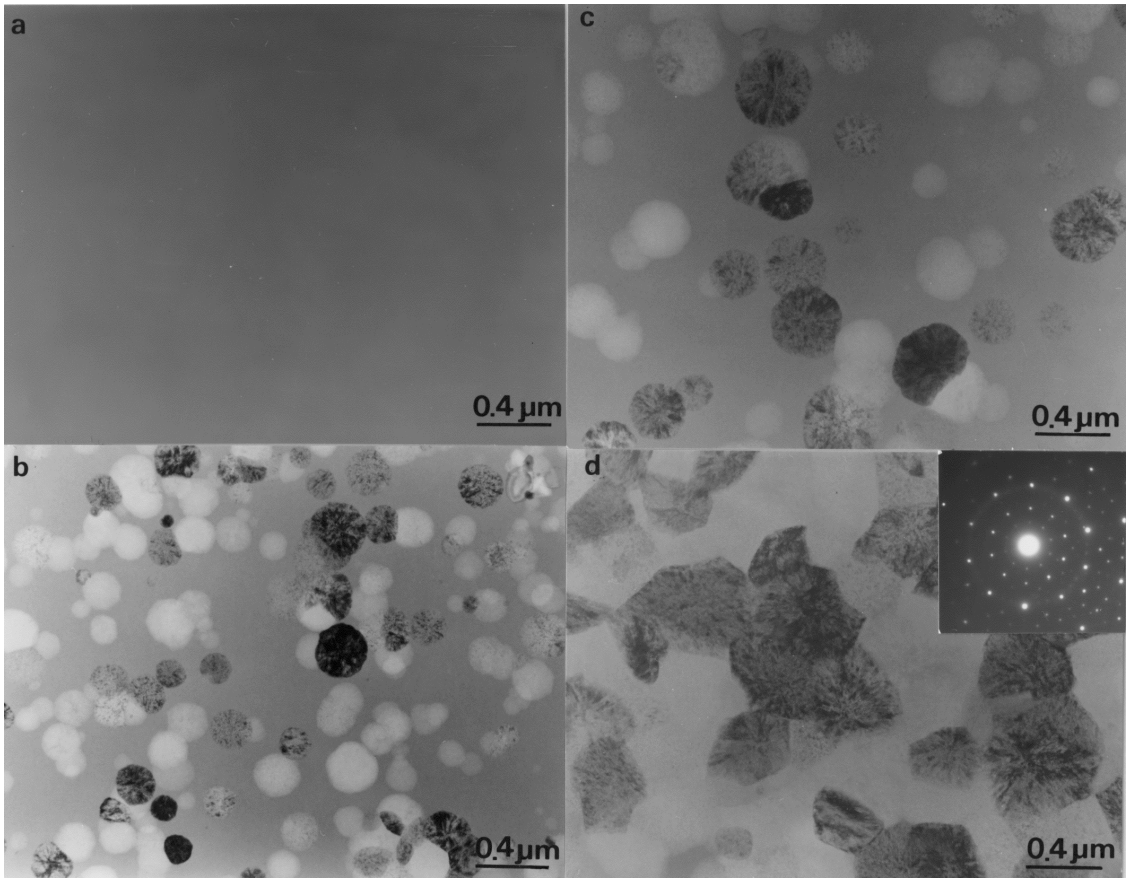

Figure 7. Evolution of crystallization to the iQc for the $Al_{75}Cu_{15}V_{10}$ amorphous phase.

spots in the diffraction pattern (figures 8(b)–(d)) do not show deviation from the ideal positions or distortion in shape. This is further confirmed by the convergent beam (with a 10 nm diameter area) electron diffraction pattern taken along a fivefold direction and shown in figure 10, in which no visible deviation of spots from fivefold symmetry positions is observed. This is an indication that phason disorder isotropically distributed in the structure of the iQc. These observations all support the idea that the structure of the iQc obtained by the crystallization from the amorphous phase is a good example of the icosahedral glass model.

The prototype of the icosaheral glass model in three dimensions was first proposed by Shechtman and Blech [43] in an attempt to interpret the diffraction pattern from the Al–Mn iQc. Stephens and Goldman further developed this model and, in particular, considered the origin of peak broadening in the diffraction pattern [44]. The icosahedral glass models simulated with the growth algorithm have been discussed in detail, where models based on various linkages of icosahedral clusters, i.e. edge-packed, vertex-packed and face-packed, were proposed. These models all predicted the dependence of peak widths on $G_\perp{}^n$ with n around 2–2.5 [50], whereas the phason strain model predicted linear $G_\perp$ dependence of peak widths [50].

Figure 11 shows the experimental data for powder x-ray peak widths as a function of $G_\perp$ for the iQc crystallized from the amorphous phase in $Al_{53}Mn_{20}Si_{27}$ and $Al_{75}Cu_{15}V_{10}$ alloys [51] and for a stable AlCuFe quasicrystal prepared by normal solidification with consequent annealing. The dependence on $G_\perp$ is observed for the Al–Mn–Si and Al–Cu–V samples but not for the Al–Cu–Fe sample. However, because of the limited accuracy of the data, it is difficult to assert which model fits the former two samples well. For the Al–Cu–Fe sample, there is no clear dependence on $G_\perp$ since the sample is almost free of phason disorder. A promising way of producing icosahedral glass is to incorporate a more realistic growth process in which the basic packing algorithm allows the attachment of new icosahedral clusters to the existing assembly at any available face. This is similar to the aggregation model for fractal growth. One can constrain the assembly to grow in concentric shells, so that all available sites within the same radius of the initial seed must be filled before the attachments at a larger radius are allowed. In this sense, it is an isotropic (spherical) growth in which the compositions before and after growth are expected to be the same. This is in agreement with what we observed [51] in the growth process. By applying some modifications, Robertson and Moss extended the random cluster growth model and successfully explained the experimentally observed linear dependence on $G_\perp$ [52]. Therefore, the best model for describing the structure of the iQc is a modified icosahedral glass model.

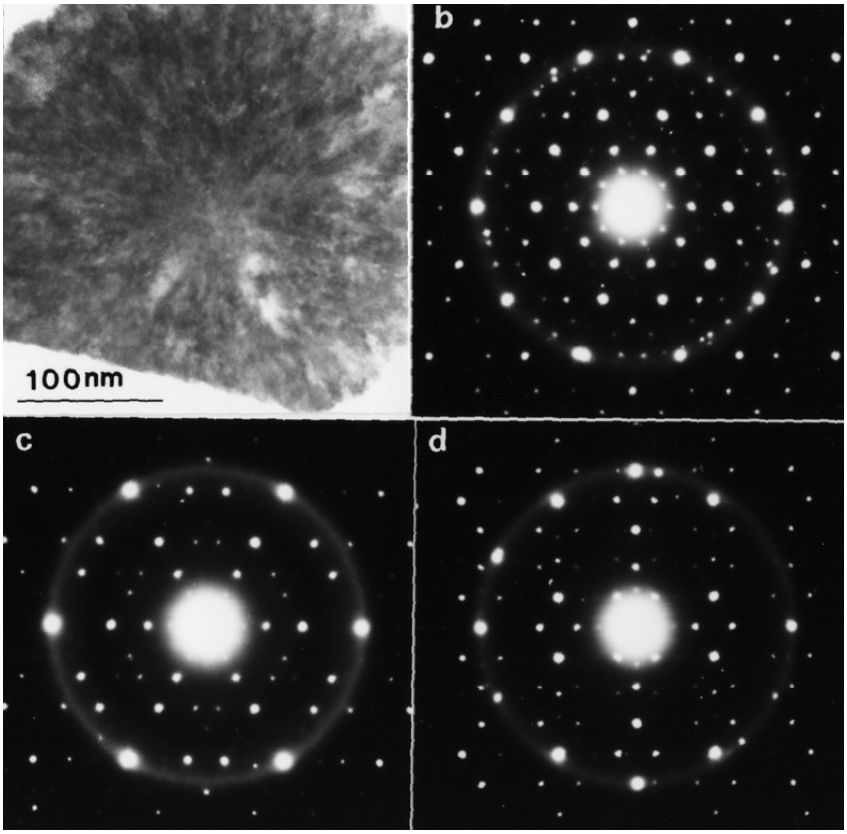

Figure 8. (a) Bright-field image and (b)–(d) electron diffraction patterns for the iQc crystallized from the amorphous $Al_{53}Si_{27}Mn_{20}$ alloy.

3.3. Quenched-in phason disorder and chemical order in Al–Cu–Fe and Al–Pd–Mn

So far, we have discussed the phason strains observed in real iQcs prepared by rapid solidification and by crystallization from an amorphous phase. In both cases, the iQcs are metastable and formed only when accompanied with phason disorder introduced during the growth processes. In this sense, the phason disorder keeps the overall structure of iQc at an icosahedral symmetry. The nature of phason disorder strongly depends on the growth process; anisotropic and fast solidification facilitates the formation of linear phason strain, as seen in the AlPdCr sample, and growth in an amorphous solid leads to isotropic phason strain or random phason strain as seen in the AlCuV and AlSiMn samples. On the other hand, since the stable AlCuFe iQc was fully annealed at high temperatures where most phason disorder had been annealed out, the diffraction peaks revealed peak widths comparable to the instrumental resolution. High resolution x-ray measurements reveal that the peak widths of the stable AlCuFe and AlCuRu iQc [16] have negligible dependence on $G_\perp$. Previous diffraction studies on $Al_{72}Pd_{25}Cr_3$ have shown that the phason strain in this sample correlates with the growth direction and is frozen into the structure as the overall form of the sample. Hiraga *et al* observed phason strain in as-cast, unannealed samples of AlCuRu [53]. The cases described above state that the phason disorder undoubtedly arises in the growth process.

On the other hand, the stable iQc in $Al_{70}Pd_{20}Mn_{10}$ alloy is slightly different from those in AlCuFe and AlCuRu alloys. Figure 12 shows partial x-ray diffraction patterns for (a) $Al_{70}Pd_{20}Mn_{10}$ and (b) $Al_{63}Cu_{25}Fe_{12}$ alloys in melt-quenched and annealed states. Evidence of phason disorder in the quenched sample of $Al_{63}Cu_{25}Fe_{12}$ is seen in the large peak widths, which are very small in the annealed sample. In contrast, the peak widths are almost the same for both quenched and annealed states for $Al_{70}Pd_{20}Mn_{10}$ alloy. The results of detailed analysis of $Al_{70}Pd_{20}Mn_{10}$ alloy are given in figure 13, where the dependence of peak widths (HWHM) on $G_\perp$ for as-quenched and annealed states is shown. The figure clearly shows that the peak widths remain at a nearly constant value of $0.0025\,\text{Å}^{-1}$ independent of $G_\perp$, in contrast to the linear increase in the peak width reported for as-quenched Al–Cu–Fe [54]. Actually, phason disorder is closely related to chemical order in the Al–Cu–Fe sample. The peak of 1/2(311111) in figure 12, which is a superlattice peak and characteristic of the structure of the face-centered icosahedral (FCI) phase, is faint in the quenched sample but becomes very strong after subsequent annealing. The diffraction pattern of the iQc without the 1/2(311111) peak is regarded as that of a simple icosahedral phase (SI). The appearance and absence of this peak indicates some sort of order–disorder transformation [55]. With this in mind, we can recognize that the increase in the intensity of the 1/2(311111) peak is always accompanied by a sharpening of diffraction peaks. This indicates that chemical ordering concurrently occurs with the relaxation of phason disorder. On the other hand, there is little difference in peak widths among all diffraction peaks and in the intensity of the 1/2(311111) peak between

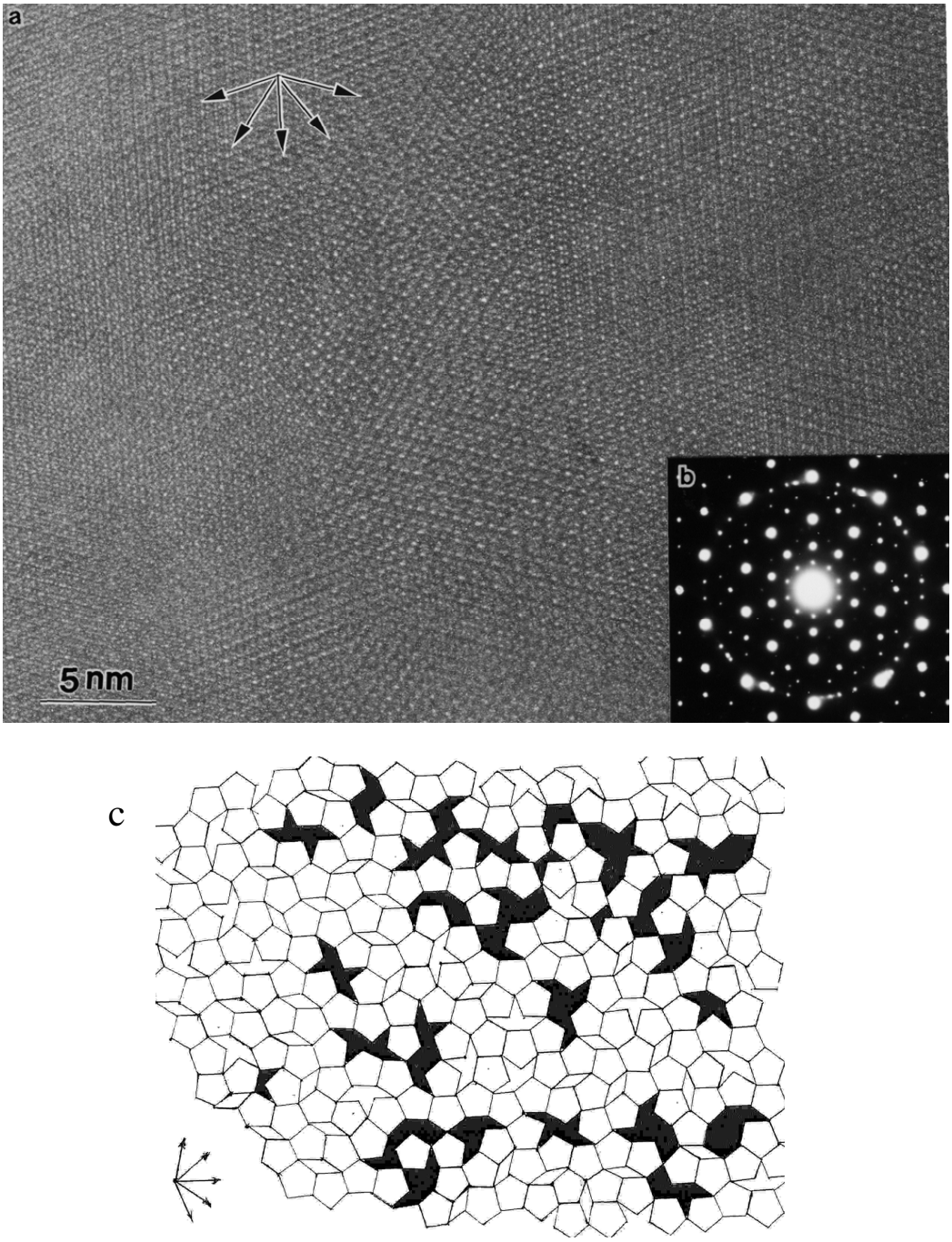

Figure 9. (a) High resolution image and (b) the corresponding electron diffraction pattern, taken along a fivefold axis from the $Al_{75}Cu_{15}V_{10}$ iQc. (c) Illustration of tiling traced from (a).

the quenched sample and the annealed sample for the iQc in the $Al_{70}Pd_{20}Mn_{10}$ alloy. This can be explained by the difference in their phase diagrams. The iQcs of both AlCuFe and AlPdMn alloys crystallize from melt via peritectic reactions. The temperature interval between liquidus and peritectic temperatures at the stoichiometric composition of the iQc is about $\sim$150 K for the Al–Cu–Fe system and $<$20 K for the Al–Pd–Mn system. The large temperature interval corresponds to the region of the $Al_{13}Fe_4$ phase and consequently, at the stoichiometric composition of the iQc ($Al_{63}Cu_{25}Fe_{12}$), $Al_{13}Fe_4$ primarily nucleates [56], indicating that a considerable concentration fluctuation exists in the melt of $Al_{63}Cu_{25}Fe_{12}$. On the other hand, with a small temperature interval, the melt of Al–Pd–Mn alloy may pass by crystallization even in small undercooling. Neutron diffraction experiments performed on an Al–Pd–Mn alloy showed that the melt exists in thermodynamical equilibrium with the iQc phase, where the structure factor of the melt just above the melting point and that of the solid are closely related [57]. The results imply that a strong chemical order already exists in the liquid state, which persists in the solid state through melt-quenching. A convergent-beam electron diffraction (CBED)

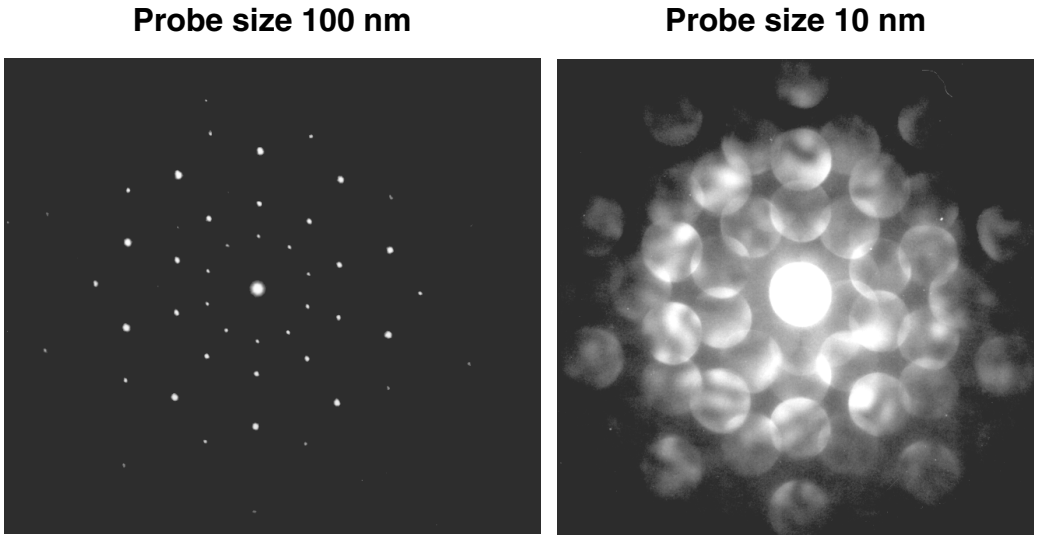

Figure 10. Selected electron diffraction and convergent-beam electron diffraction patterns taken along a fivefold axis from the $Al_{75}Cu_{15}V_{10}$ iQc.

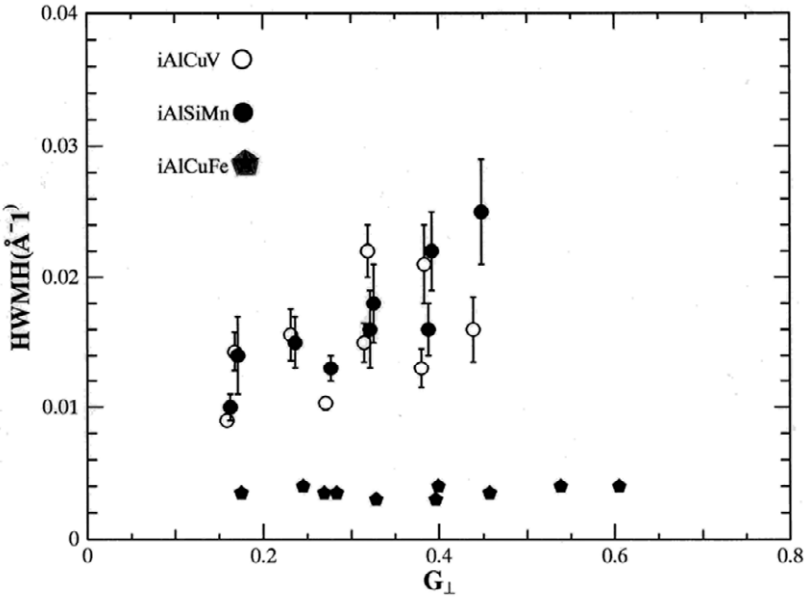

Figure 11. $G_\perp$ dependence of peak widths for the $Al_{75}Cu_{15}V_{10}$ and $Al_{53}Si_{27}Mn_{20}$ iQcs.

study revealed that fully annealed stable iQc $Al_{70}Pd_{20}Mn_{10}$ exhibits a overall long-range structure better than that of the melt-quenched sample, but the melt-quenched sample still displays the best local structure [58].

3.4. Phason disorder and chemical compositions (Al–Pd–Mn)

In the previous section, it was shown that the occurrence of phason strain in the iQc strongly depends on the chemical order. The iQc with a composition deviating from stoichiometry always manifests considerable phason strain, as evidenced by the peak broadening [59], while diffraction peaks of the stable iQc are very sharp and appear to be the same in fully annealed and melt-quenched samples. $Al_{74}Pd_{17}Mn_9$ alloy, which slightly deviates from the stoichiometry of the iQc, is a single iQc phase in the melt-quenched state, which is somewhat stable even at 863 K, whereas the single phase decomposes to a mixture with a new iQc phase and a few crystalline phases after annealing at 1073 K, as shown in figure 14. Figure 15 shows bright-field images and fivefold diffraction patterns for $Al_{74}Pd_{17}Mn_9$ (a,c) in the melt-quenched state and (b,d) in the annealed state. In comparison with the iQc of the $Al_{70}Pd_{20}Mn_{10}$ sample, the melt-quenched $Al_{74}Pd_{17}Mn_9$ reveals broader peak widths. After annealing at 1073 K, concurrent with annihilation of phason strain corresponding to a drastic peak sharpening, the precipitation of crystalline phases occurs. The precipitation of the crystalline phases is an indication that a change in composition of the iQc phase might occur upon annealing. Energy-dispersed x-ray (EDX) analysis verified the composition to be $Al_{74}Pd_{18}Mn_8$ for the as-quenched sample and $Al_{72}Pd_{20}Mn_8$ for the iQc

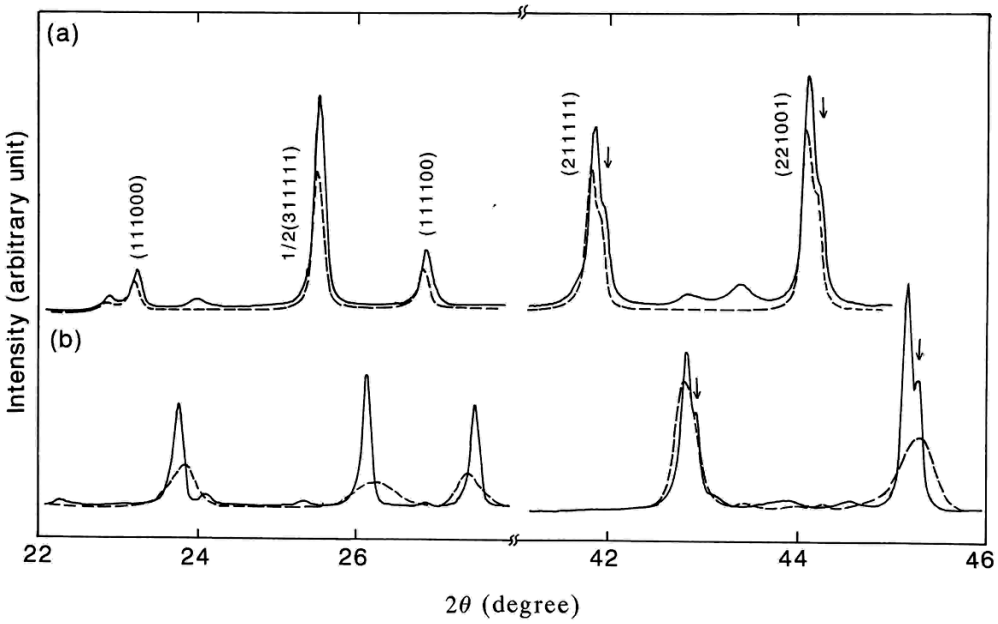

Figure 12. Powder x-ray pattern of iQcs in the as-quenched state (dotted lines) and annealed state (solid lines) for (a) $Al_{70}Pd_{20}Mn_{10}$ and (b) $Al_{63}Cu_{25}Fe_{12}$ iQcs.

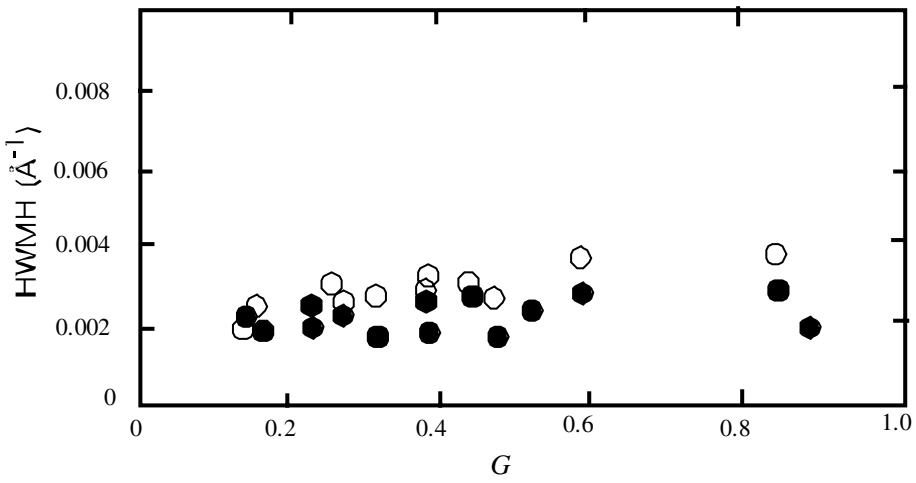

Figure 13. $G_{\perp}$ dependence of peak widths for the as-quenched and annealed $Al_{70}Pd_{20}Mn_{10}$ iQcs.

region after annealing. The difference in the composition of the $Al_{74}Pd_{17}Mn_9$ sample between as-quenched and fully annealed states suggests that the annihilation of phason strain occurs through a composition change in the iQc phase owing to the precipitation of crystalline phases. In TEM observations, it is clear that all precipitates nucleate at grain boundaries and grow into iQc grains via a long-range diffusion of Al/Pd. Since the nominal composition of the sample is slightly lower in Pd compared with stoichiometry, Pd and Al atoms will diffuse across the interface into the iQc phase and into the crystalline phases, respectively, during diffusion. The long-range diffusion of Al and Pd atoms is the driving force behind the elimination of the phason disorder. This is in good agreement with a report [60] that phason disorder is strongly dependent on the composition represented by the ratio of Al/Pd. For an alloy with a composition deviating slightly from stoichiometry, e.g. melt-quenched $Al_{75}Pd_{15}Mn_{10}$ consisting of an iQc phase with a large amount of phason disorder, will trasform entirely to crystalline phases upon annealing. By summarizing the results, a free energy-composition diagram is obtained and shown in figure 16 [60]. As long as temperature is finite, it is possible to have a finite composition for the stable iQc, as shown in figure 16. The stoichiometric composition of the stable iQc (or phason-free iQc) is in a narrow range, while the melt-quenched (metastable or phason-in iQc) iQc is formed over a wide composition range. According to the phase diagram of Al–Pd–Mn systems, there are several intermetallic phases existing at compositions in the vicinity of the iQc composition. If an alloy has a composition very close to that of the stable iQc, e.g. denoted as C_1, the difference in energy between phason-containing and phason free iQcs, ΔG_1, would be small. Here, ΔG_1 corresponds to the energy consumed in the decomposition of phason-containing iQc into the phason-free and crystalline phases. In contrast, if an alloy has

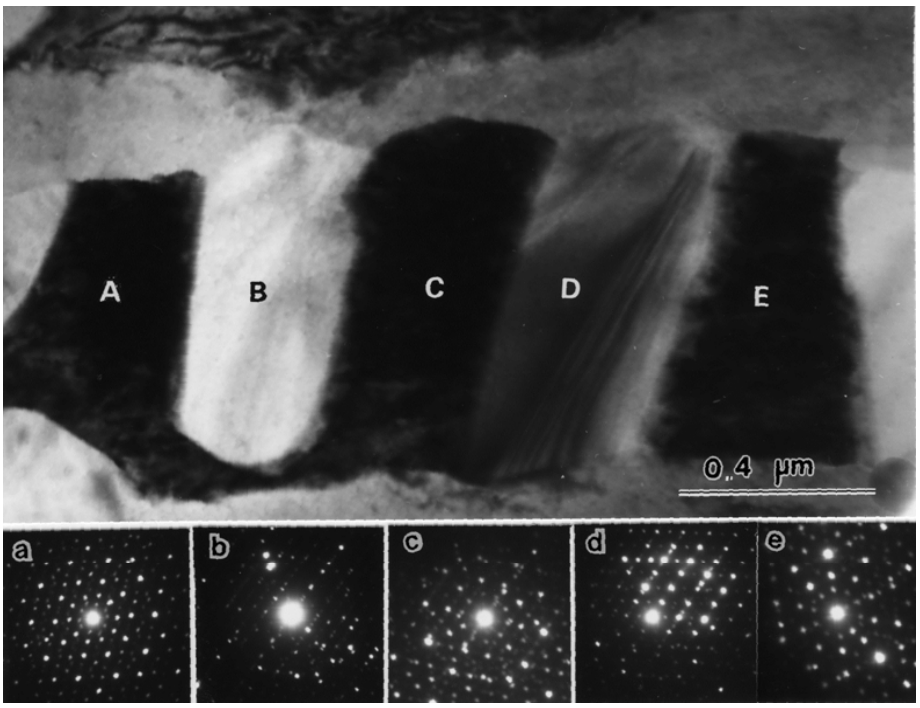

Figure 14. Crystallization of melt-quenched $Al_{74}Pd_{17}Mn_9$ annealed at 1503 K for 24 h.

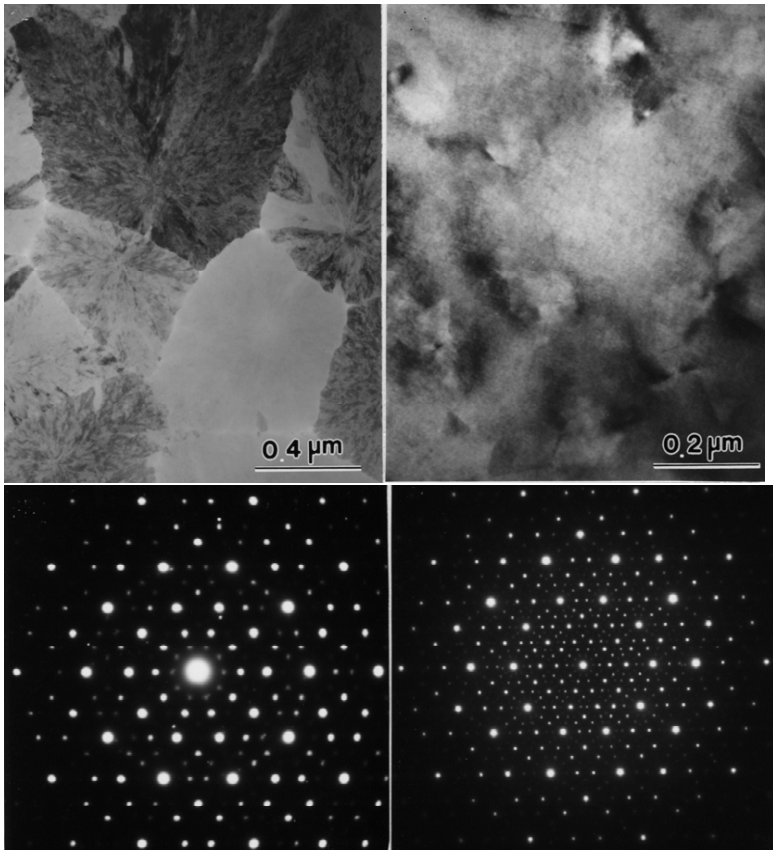

Figure 15. Bright-field images and fivefold diffraction patterns before and after annealing for melt-quenched $Al_{74}Pd_{17}Mn_9$.

a composition far from the stoichiometric one, e.g. denoted as C_2, the difference in energy, ΔG_2, will be significantly large. For alloys with compositions in this region, the phason-free iQc phase is not expected to be formed even upon full annealing, i.e. no equilibrium iQc phase exists. This again demonstrates that the stable iQc is determined by the composition of the alloy itself. As stated in the last section, the stoichiometric iQcs prepared by melt-quenching and by full

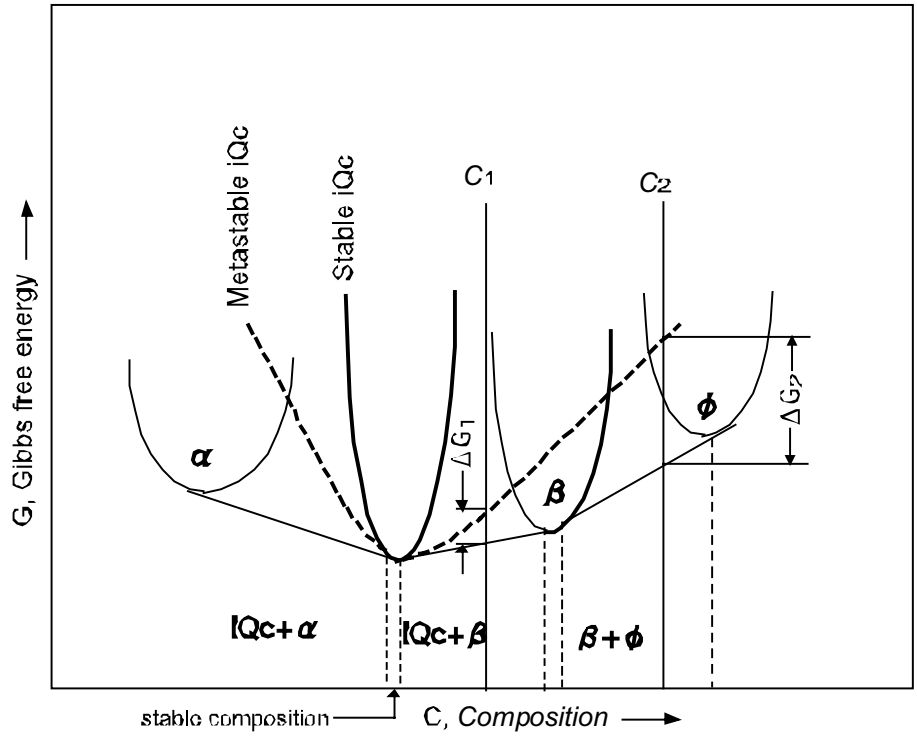

Figure 16. Schematic of free-energy composition for the iQc and crystalline compounds. Metastable iQc shown by broken line represents the region of the melt-quenched iQc.

annealing are similar with respect to peak widths, while a drastic peak broadening occurs if the composition of the sample is off-stoichiometry. Therefore, the off-stoichiometry iQc is thermodynamically unstable and generally contains a certain amount of phason disorder.

4. Hume-Rothery conditions for stable iQcs

The stable iQcs are those are in equilibrium states within certain temperature ranges and exist in equilibrium phase diagrams. Like crystals, stable iQcs with sizes of centimeter order can be grown by conventional crystal growth techniques, they generally have high perfection of their structures. Similar to those in intermetallic compounds, almost stable iQcs form at narrow range of compositions, and therefore, their stability can be discussed using Hume-Rothery rules. Table 2 summarizes typical stable iQcs that have been identified so far. Hume-Rothery deduced a series of rules [6] that identify factors favoring the formation of definite phases within certain concentration ranges of noble-metal-based binary alloys. These factors are size, eletronegativity and valence electron concentration. We discuss the stability of iQcs with respect to Hume-Rothery conditions, i.e. the valence electron concentration and the atomic size factor, and compare the iQcs of the Cd–RE class with those of the Al–Mn–Si and Mg–Zn–Al classes. A detailed discussion has been given in [61].

4.1. Valence electron concentration

The valences of transition metals (TM) used here are determined on the basis of Pauling's phenomenological theory [62]. According to Pauling, the 3d and 4s orbitals must be considered as a whole when assessing the nature of bonding. He suggested that of these electrons, approximately 5.78 per atom are concerned with bonding, while the remainder occupy a band of energy levels, which are called as Pauling atomic orbitals. There are 2.44 atomic orbitals, each of which can accommodate one electron of positive spin and one electron of negative spin. The electrons occupying the atomic orbitals, however, tend to remain unpaired as long as possible, i.e. to have no corresponding electron of opposite spin. Thus, Cr with 6 electrons outside the argon-like core has 5.78 bonding electrons and 2.22 unpaired electrons in atomic orbitals. Mn, with one electron more, has 1.22 unpaired electrons in atomic orbitals, while Fe has 2.22 unpaired electrons. Since there are 2.44 atomic orbitals, there is room for 2.44 unpaired electrons, consequently for Co, with one electron more than Fe, the pairing of electrons of opposite spins must begin. For Ni, yet another electron induces further pairing. The number of atomic orbitals was deduced from the saturation magnetic moment of Fe and its alloys. The saturation of the magnetic moment of Fe is 2.22 Bohr magnetons per atom. When Co is dissolved in Fe, the number of electrons to be accommodated in atomic orbitals increases, and experimentally, it has been found that the first additions raise the saturation magnetic moment to a maximum of 2.44 Bohr magnetons per atom, after which, further additions cause a decrease. Thus, the number of unpaired atomic orbital electrons can increase to 2.44 per atom, but further electrons must pair with those already present. Therefore, the atomic orbitals could be represented as being divided into two compartments in which electrons with opposite spin quantum numbers can be accommodated,

Table 2. Type of structure for stable.

	P-type	F-type
Al–Mn–Si		$Al_{63}Cu_{25}TM_{12}$(TM:Fe Ru Os) $Al_{70}Pd_{20}TM_{10}$(TM:Mn Tc Re)
Zn–Mg–Al	Al_5Li_3Cu $Zn_{70}Mg_{20}RE_{10}$(RE:Er Ho)	$Zn_{60}Mg_{30}RE_{10}$(RE:Y Dy Ho Gd Er Tb) $Zn_{74}Mg_{19}TM_7$(TM:Zr Hf)
Cd–Yb	$Cd_{5.7}M$(M:Yb Ca) $Cd_{65}Mg_{20}M_{15}$(M:Yb Ca Y Ho Gd Er Tb) $Zn_{80}Mg_5Sc_{15}$ $In_{42}Ag_{42}M_{16}$(M:Yb Ca) $Zn_{74}Ag_{10}Sc_{16}$, $Zn_{75}Pd_9Sc_{16}$ $Zn_{77}Fe_7Sc_{16}$, $Zn_{78}Co_6Sc_{16}$ $Zn_{75}Ni_{10}Sc_{15}$	

Table 3. Electron distribution for Cr, Mn, Fe, Co and Ni. Redrawn from [63].

Metals	Cr	Mn	Fe	Co	Ni
Configuration in free atom	(2) (2,6) (2,6,5) 1	(2) (2,6) (2,6,5) 2	(2) (2,6) (2,6,6) 2	(2) (2,6) (2,6,7) 2	(2) (2,6) (2,6,8) 2
Electrons in bonding orbitals	5.78	5.78	5.78	5.78	5.78
Unpaired electrons in atomic orbitals	0.22	1.22	2.22	1.71	0.61
Paired electrons in atomic orbitals	———	———	———	1.51	3.61
Total electrons	6	7	8	9	10
Number of vacancies in atomic orbitals	*4.66*	*3.66*	*2.66*	*1.71*	*0.61*
Distribution of electrons in atomic orbitals	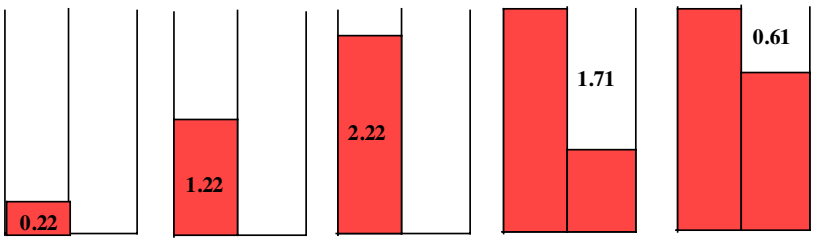				

as shown in table 3. Under this assumption, the number of unpaired electrons for Co and Ni is 1.66 and 0.66, respectively; the actual saturation magnetic moments are 1.71 and 0.61. Therefore, Cr, Mn, Fe, Co and Ni have, respectively, 4.66, 3.66, 2.66, 1.61 and 0.71 vacancies per atom in the atomic orbitals. It appears probable that, in alloys, these vacancies are filled by electrons contributed by the counterpart element, particularly when it has a high valency. Using those values, Raynor succeeded in explaining the formation of Al–TM binary compounds, except for Al_3Fe [63]. The same values have been applied for the iQcs. In this class, a stable iQc forms for $Al_{63}Cu_{25}TM_{12}$, where TM = Fe, Ru or Os, and for $Al_{70}Pd_{20}TM_{10}$, where TM = Mn, Tc or Re as shown in figure 17. It is interesting to note that Fe, Ru, Os and Mn, Tc, Re are located in the same columns of the periodic table and the iQc forms at different stoichiometry in the two systems, but keep the same value of e/a (e/a: electron to atom ratio or valence electron concentration). These are indications that the value used for this group is appropriate. Thus, the stable iQcs in the Al–Mn–Si class have the same e/a value, namely, ∼1.75 [61].

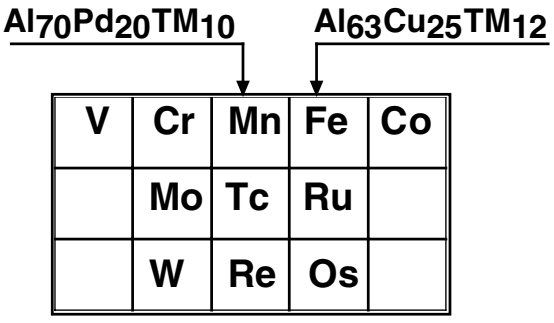

Figure 17. Formation of stable iQc in the Al–Cu–TM and the Al–Pd–TM systems.

Assigning negative valencies for TM elements in Al–TM alloys has been controversial, but the important point is that the use of these values led to the discovery of a number of stable iQcs. Recently, these values were estimated to be positive in some complex Zn–TM and Al–V alloys [64] and Zn–TM–Sc iQcs [31]. However, to date, there are still

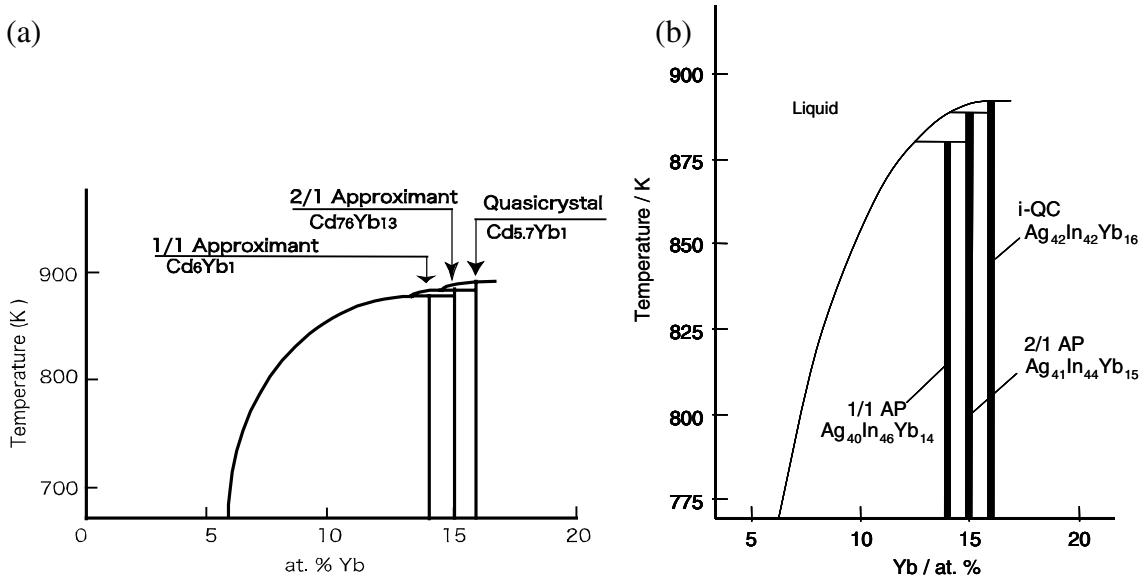

Figure 18. (a) Binary Cd–Yb phase diagram and (b) pseudobinary In–Ag–Yb phase diagram involving iQc.

no available values for Fe and Mn in Al–TM alloys. It is highly interesting that the effective e/a for Ru derived from an Al–Cu–Ru–Si approximant is ∼0.76 [65]. If we apply this value to $Al_{63}Cu_{25}Ru_{12}$, we obtain an average e/a of ∼2.13 for the stable iQc, and the iQcs of the AlMnSi class would fall into the AlZnMg and Cd–Yb classes.

The physical meaning of the Hume-Rothery condition of the definite e/a for the stable iQcs is interpreted in terms of the formation of the pseudogap across the Fermi level as a result of an interaction between Fermi sphere and Brillouin zone [66]. The observation of the smallest electron specific heat coefficient (γ) for a stable AlCuRu iQc among a number of Al-based alloys is evidence supporting the above-mentioned speculation [67]. Stability in this viewpoint had been applied to approximants and several complex alloys and has been reviewed in three articles [65, 68, 69].

Apart from the Al–Mn–Si class in which the stable iQcs shows a narrow range of e/a of 1.75, those in the Mg–Zn–Al and Cd–Yb classes exhibit more flexible e/a ranging from 2.0 to 2.15. However, the stable iQcs formed in $Zn_{60}Mg_{30}RE_{10}$ systems with different REs but the same composition have the same e/a of 2.15. Furthermore, replacement of Cd by half In and half Ag for the stable $Cd_{84}Yb_{16}$ and $Cd_{84}Ca_{16}$ iQcs led to the formation of the stable $In_{42}Ag_{42}Yb_{16}$ and $In_{42}Ag_{42}Ca_{16}$ iQcs [30]. The Yb atoms in the iQcs have been verified to be divalent, and therefore, e/a for the stable $Cd_{84}Yb_{16}$ and $Cd_{84}Ca_{16}$ iQcs, as well as for the $In_{42}Ag_{42}Yb_{16}$ and $In_{42}Ag_{42}Ca_{16}$ iQcs, is 2.0. It is surprising to see in figure 18 that the iQc and the 2/1 and 1/1 approximants formed in a narrow composition region in the binary phase diagram of the Cd–Yb system also exist in the pseudo-binary phase diagram of the In–Ag–Yb system [70]. The replacement of Cd by In and Ag is possible not only for iQc but also for the 2/1 and 1/1 approximants. This is further solid evidence that e/a is the most prominent factor in governing the stability of the quasicrystalline structure.

4.2. Atomic size factor

The atomic size factor of an alloy containing A and B elements is defined as $\delta = (r_A - r_B)/r_A$ where r_A and r_B are the atomic radii of atoms A and B, respectively. For the Al–Mn–Si class, iQcs are formed within a very narrow compositional range with e/a limited between 1.7 and 1.8. A slight change in composition would result in the formation of crystalline phases. In this class, e/a is the dominant factor in the formation of the iQc.

For the Zn–Mg–Al class, the stable iQc shows a solubility range. The replacement of Zn by Mg reaches 5 at.% in this iQc, which induces an expansion in the lattice, as observed in x-ray diffraction patterns, confirming the dissolution of Mg into the quasicrystalline structure. The value of δ for Zn/Mg is about 15%, which corresponds to the limits of the solubility. The importance of the atomic size of the RE element to phase formation in this class is reflected in the observation that the stable iQcs are formed in alloys containing RE elements with atomic radii in the range of 0.173–0.179 nm.

For the Cd–Yb class, the iQc has a high solubility of Mg. It has been reported that the formation range of the iQc expands towards the Mg-rich side [71]. The iQc forms even when Cd is replaced with 60 at.% Mg. The δ for Cd/Mg is 2% and this allows for a large replacement of Cd by Mg.

4.3. Different constrains among groups

The stability and range of solubility of the iQcs could be clarified within the framework of the Hume-Rothery rules. However, the criteria are slightly different among the three groups.

The first priority of the criterion for the formation of iQcs is e/a. This is definitely rigid and even stricter than in the case of the electron phases that were studied by Hume-Rothery [6], and thus it turns out to be characteristic of stable iQcs. The fact that the formation of Cd–Yb and Cd–Ca extends to In–Ag–Yb and In–Ag–Ca ternary alloys indicates the importance of e/a.

The low solubility of the stable iQcs of the Al–Mn–Si class is due to a significant difference in valence among the constituent elements. For example, the replacement of an Al by one Fe atom will induce a decrease of 5.66 electrons. A slight change in composition results in a large deviation of e/a. This explains the low solubility and the narrow composition range of the iQcs in the Al–Mn–Si class. Since both Zn and Mg are divalent, an exchange between Zn and Mg does not change the e/a for the Zn–Mg–Al class, and thus a certain amount of replacement is allowed. However, when the e/a is favorable the atomic size factor will become dominant and the large δ forces the maximum solubility of Mg to be limited to less than 5 at.%. A detailed study on phase formation indicated that 2–3 at.% replacement of Y by Mg is acceptable and that the composition constraint is lower than that in the Al–Mn–Si class.

For the Cd–Yb class, the range of solubility (Cd/Mg replacement) in the iQc expands to 60 at.%. This can be simply explained by the similarity in both the valence and the atomic size factor between Cd and Mg. The Cd/Mg replacement first preserves the e/a criterion and leads to a small δ of only $\sim$2%. The product of δ and solubility is a measure of the distortion due to atom replacement. For smaller δ, a larger solubility is expected. A small amount of Yb replacement is even allowed in this system.

5. Concluding remarks

In this review, we focused on three examples of iQcs fabricated by different processes; stable iQcs grown by slow cooling or casting with subsequent annealing, metastable iQcs prepared by melt-spinning, and metastable iQcs formed by the crystallization of the amorphous phase. The stability was discussed in terms of Hume-Rothery rules for the stable iQcs and in terms of phason disorder for metastable iQcs. The roles of composition and chemical order were also discussed in relation to phason disorder.

It seems that the origin of the stabilization mechanism is different for the stable and metastable iQcs. Nevertheless, there is a common feature observed in most iQc-forming alloy liquids or their undercooled liquids: a local icosahedral order. For a stable AlPdMn iQc, the icosahedral order was observed in the ***liquid state*** just above the melting temperature [57]. For a metastable Al–Mn iQc the icosahedral order was observed in the ***undercooled liquid state*** [66]. Icosahedral orders observed in amorphous AlCuV and AlMnSi alloys are another proof that icosahedral order does exist in the undercooled liquid. Recently, there was an interesting report of the observation of an enhanced icosahedral short-range order with undercooling in $Ti_{39.5}Zr_{39.5}Ni_{21}$ liquids which form iQcs upon rapid solidification, in an electrostically levitated droplet [67]. Figure 19 shows (a) cooling curves of the liquids and (b) the diffraction patterns in each cooling stage. There are two recalescence events in the cooling curves for the undercooled liquids: the 1st recalescence is responsible for the transition of the iQc and the 2nd one is the transition to a C14 (Laves) phase. This is the first direct evidence that verifies Frank's hypothesis [68]. It was also reported

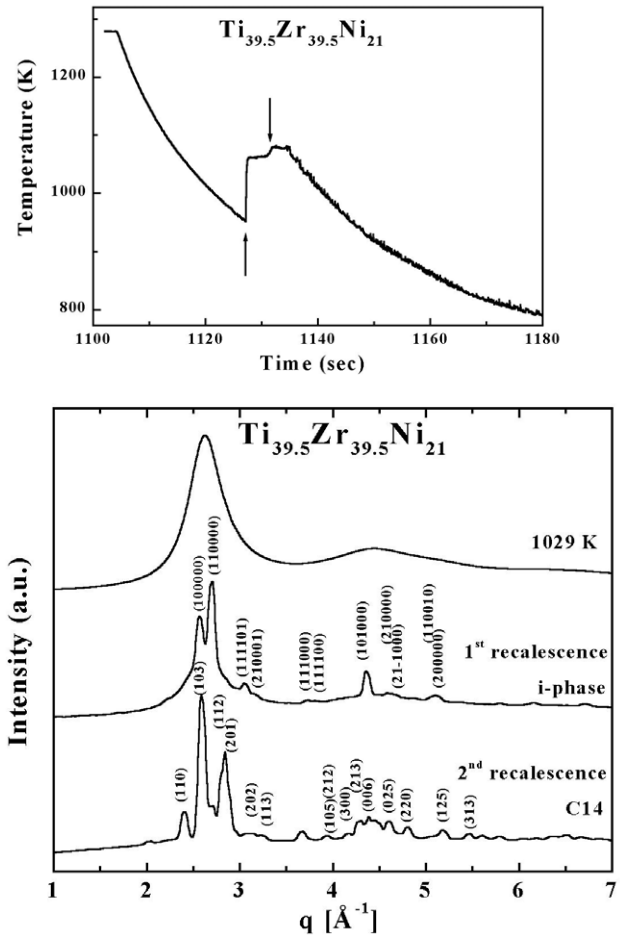

Figure 19. (a) Cooling curves for electostatically levitated droplet of Ti–Zr–Ni as a function of temperature. (b) X-ray diffraction pattern as a function of q vector ($q = 4\pi \sin\theta/\lambda$) for undercooled Ti–Zr–Ni alloy at different temperatures corresponding to (a). [73] Courtesy of K Kelton.

that the activation energy for nucleation is lower for an icosahedral cluster than for cubic base clusters in a number of Al alloys [56]. For the same reason, we can expect to observe the icosahedral order in undercooled liquids of the Al–Pd–Cr alloys. For simplicity, we can say that the icosahedral order is in equilibrium in the ***liquid state*** for the stable iQcs, whereas the icosahedral order prevails in the ***undercooled liquid state*** for the metastable iQcs. The stability and the density of the icosahedral order in liquids govern which phase will be formed during solidification: a metastable iQc or a stable iQc. To obtain a universal picture, approaches concerning the liquid structure of non-Al-based iQc-forming alloys are highly promising.

Acknowledgments

The author is grateful to Professor Ken Kelton at Washington University for providing figure 19. I also thank Dr Krishanu Biswas for stimulating discussion and reading the manuscript. This work was supported in part by Grants-in-Aid for Scientific Research (A) 19206072 from Ministry of Education, Culture, Sports, Science and Technology.

References

[1] Shechtman D, Blech I, Gratias D and Cahn J W 1984 *Phys. Rev. Lett.* **53** 1951
[2] Kittel C 2004 *Introduction to Solid State Physics* (Hoboken, NJ: Wiley)
[3] Tsai A P 1999 *Physical Properties of Quasicrystals* ed Z M Stadnik (Berlin: Springer)
[4] Tsai A P 2003 *Acc. Chem. Res.* **36** 31
[5] Zeng X, Ungar G, Liu Y, Percec V, Dulcey A E and Hobbs J K 2004 *Nature* **428** 157
[6] Hume-Rothery W 1926 *J. Inst. Metals* **35** 295
[7] Steinhardt P J and Ostlund S 1987 *The Physics of Quasicrystal* (Singapore: World Scientific)
[8] Levine D and Steinhardt P J 1986 *Phys. Rev.* B **34** 596
[9] Socolar J E S, Lubensky T C and Steinhardt P J 1986 *Phys. Rev.* B **34** 3345
[10] Stephens P W and Goldman A I 1991 *Sci. Am.* April 44
[11] Kaneko Y, Maezawa R, Kaneko H and Ishimasa T 2002 *Philos. Mag. Lett.* **82** 483
[12] Yamamoto A, Takakura H and Tsai A P 2003 *Phys. Rev.* B **68** 94201
[13] Takakura H, Gomez C P, Yamamoto A, de Boissieu M and Tsai A P 2007 *Nat. Mater.* **6** 58
[14] de Bruijn N 1985 *Ned. Akad. Weten. Proc. Ser.* A **43** 39
[15] Elser V 1985 *Acta Cryst.* A **42** 36
[16] Guryan C A, Goldman A I, Stephens P W, Hiraga K, Tsai A P, Inoue A and Masumoto T 1989 *Phys. Rev. Lett.* **62** 2409
[17] Deng B B and Kuo K H 2004 *J. Alloys Compounds* **366** L1
[18] Rokhsar J L, Wright D C and Mermin N D 1986 *Phys. Rev.* B **35** 5487
[19] Cahn J W, Shechtman D and Gratias D 1986 *J. Mater. Res.* **1** 13
[20] Ishimasa T, Fukano Y and Tsuchimori M 1988 *Philos. Mag. Lett.* **58** 157
[21] Ebalard S and Spaepen F 1989 *J. Mater. Res.* **4** 39
[22] Tsai A P, Guo J Q, Abe E, Takakura H and Sato T J 2000 *Nature* **408** 537
[23] Elser V and Henley C L 1985 *Phys. Rev. Lett.* **55** 2883
[24] Cooper M and Robinson H 1966 *Acta Crystallogr.* **20** 614
[25] Bergman G, Waugh J L T and Pauling L 1954 *Acta Crystallogr.* **10** 254
[26] Henley C L and Elser V 1986 *Philos. Mag.* B **53** 59
[27] Palenzona A 1971 *J. Less-Common Met.* **25** 367
[28] Mizutani U, Takeuchi T and Sato H 2002 *J. Phys.: Condens. Matter* **14** R767
[29] Sugiyama K and Hiraga K 1998 *Zeit. Kristallogr.* **213** 168
[30] Guo J Q, Abe E and Tsai A P 2002 *Philos. Mag. Lett.* **82** 27
[31] Maezawa R, Kashimoto Y and Ishimasa T 2004 *Philos. Mag. Lett.* **84** 215
[32] Socolar J E S and Wright D C 1987 *Phys. Rev. Lett.* **59** 221
[33] Tanaka M, Terauchi M, Hiraga K and Hirabayashi M 1985 *Ultramicroscopy* **17** 279
[34] Bancel P A and Heiney P A 1986 *J. Phys.* (Colloque C3) **47** C3-341
[35] Lubensky T C, Socolar J E S, Steinhardt P J, Bamcel P A and Heiney P A 1986 *Phys. Rev. Lett.* **57** 1440
[36] Follstaedt D M and Knapp J A 1989 *J. Mater. Res.* **4** 1398
[37] Mukhopadhyay N K, Ishihara K N, Ranganathan S and Chattopadhyay K 1990 *Acta Metall. Mater.* **39** 1151
[38] Ma L, Wang R and Kuo K H 1988 *Scr. Metall.* **22** 1791
[39] Sun W, Yubuta K and Hiraga K 1995 *Philos. Mag.* B **71** 71
[40] Tsai A P, Inoue A, Yokoyama Y and Masumoto T 1990 *Japan. J. Appl. Phys.* **29** L1161
[41] Tsai A P, Inoue A and Masumoto T 1991 *J. Appl. Phys.* **69** 2728
[42] Steinhardt P J, Nelson D R and Ronchetti R 1984 *Phys. Rev. Lett.* **53** 1951
[43] Shechtman D and Blech I 1985 *Trans.* **16A** 1005
[44] Stephens P W and Goldman A I 1986 *Phys. Rev. Lett.* **56** 1168
[45] Tsai A P, Inoue A, Bizen Y and Masumoto T 1989 *Acta Metall.* **37** 1443
[46] Koster U, Meinhardt J, Ross S and Liebertz H 1996 *Appl. Phys. Lett.* **69** 179
[47] Brown B J 1959 *Acta Crystallogr.* **12** 995
[48] Kofalt D D, Nanao S, Egami T, Wong K M and Poon S J 1986 *Phys. Rev. Lett.* **57** 114
[49] Matsubara E, Waseda Y, Tsai A P, Inoue A and Masumoto T 1988 *Z. Naturf.* **43A** 505
[50] Horn P M, Malzfldt W, Divincenzo D P, Toner J and Gambino R 1986 **57** 1444
[51] Tsai A P, Hiraga K, Inoue A, Masumoto T and Chen H S 1994 *Phys. Rev.* B **49** 3569
[52] Robertson J L and Moss S C 1991 *Phys. Rev. Lett.* **66** 353
[53] Hiraga K, Lee K H, Hirabayashi M, Tsai A P, Inoue A and Masumoto T 1989 *Japan. J. Appl. Phys.* **28** L1624
[54] Calvayrac Y, Quivy A, Bessiere M, Lalebrre S and Cornier-Quiquandon M 1990 *J. Phys. (Paris)* **51** 417
[55] Tsai A P, Inoue A and Masumoto T 1990 *Philos. Mag. Lett.* **62** 95
[56] Holland-Moritz D, Schroers J, Herlach D M, Grushko B and Urban K 1998 *Acta Mater.* **46** 1601
[57] Klein H, Audier M, Simonet V, Hippert F and Bellissent R 1998 *Physica* B **241–243** 964
[58] Tanaka M 1991 *RITU* **36** 195
[59] Tsai A P, Chen H S, Inoue A and Masumoto T 1991 *Phys. Rev.* B **43** 8782
[60] Tsai A P, Chen H S, Inoue A and Masumoto T 1992 *Japan. J. Appl. Phys.* **31** L419
[61] Tsai A P 2004 *J. Non-Cryst. Solids* **334–335** 317
[62] Pauling L 1938 *Phys. Rev.* **54** 899
[63] Raynor G V 1949 *Prog. Met.* **1** 1
[64] Mizutani U, Asahi R, Sato H and Takeuchi T 2006 *Phys. Rev.* B **74** 235119
[65] Mizutani U, Takeuchi T and Sato H 2004 *Prog. Mater. Sci.* **49** 227
[66] Jones H 1937 *Proc. Phys. Soc. Lond.* **49** 250
[67] Mizutani U, Sakabe Y, Shibuya T, Kishi K, Kimura K and Takeuchi S 1990 *J. Phys.: Condens. Matter* **2** 6169
[68] de Laissardiere G T, Nguyen-Manh D and Mayou D 2005 *Prog. Mater. Sci.* **50** 679
[69] Ishii Y and Fujiwara T 2008 *Quasicrystals Handbook of Metal Physics* ed Y Ishii and T Fujiwara (Amsterdam: Elsevier) p 171
[70] Ohashi S, Hasegawa J, Takeuchi S and Tsai A P 2007 *Philos. Mag.* **87** 3089
[71] Guo J Q, Abe E and Tsai A P 2002 *Philos. Mag. Lett.* **82** 27
[72] Jakse N, Le Bacq O and Pasturel A 2005 *J. Chem. Phys.* **123** 104508
[73] Kelton K F, Lee G W, Gangopadhyay A K, Hyers R W, Rathz T J, Rogers J R, Robinson M B and Robinson D S 2003 *Phys. Rev. Lett.* **90** 195504
[74] Frank F C 1952 *Proc. R. Soc.* A **215** 43